Vertically sheared horizontal flow with mass sources: a canonical balanced model

Andrew J. Majda [a]; Majid Mohammadian [b]; Yulong Xing [a]
[a] Department of Mathematics and The Center for Atmosphere Ocean Science, Courant Institute of
Mathematical Sciences, New York University, New York, NY [b] Numerical Prediction Research, Environment
Canada, Dorval, Qubec, Canada

PLEASE SCROLL DOWN FOR ARTICLE

Taylor & Francis
Taylor & Francis Group

Vertically sheared horizontal flow with mass sources: a canonical balanced model

ANDREW J. MAJDA*†, MAJID MOHAMMADIAN‡ and YULONG XING†

†Department of Mathematics and The Center for Atmosphere Ocean Science,
Courant Institute of Mathematical Sciences, New York University, New York, NY
‡Numerical Prediction Research, Environment Canada, Dorval, Qubec, Canada

Canonical balanced dynamic equations involving vertically sheared horizontal flow with heat or mass sources have emerged recently in systematic multi-scale modeling of the equatorial wave guide on a wide range of spatio-temporal scales. Here, a new self-contained derivation of these equations is developed briefly in a context for potential applications to the hurricane embryo. These canonical balanced equations are studied through a combination of exact solutions and simple numerics. The results below include elementary exact solutions given by velocity fields that are linear in the spatial coordinates combined with an exact nonlinear stability analysis for vertical vorticity amplification in such a preconditioned environment. Other elementary solutions studied here include the evolution of radial eddies, which represent "hot towers" in the hurricane embryo in a suitable radial preconditioned background environment.

Keywords: Cyclogenesis; Hot towers; Strong shear sources; Vertical shear; Horizontal flows; Stability analysis

1. Introduction

Reduced models for rotating stratified flows have a central role in the understanding of geophysical and astrophysical phenomena. Perhaps, the most familiar models of this sort are the quasi-geostrophic models, which are appropriate for mid-latitudes on suitable scales and arise through geostrophic balance of Coriolis terms and pressure gradients for low Froude number flows (Pedlosky 1979, Embid and Majda 1998, Majda 2003, Julien *et al.* 2006). At the equator, the vertical projection of the planetary rotation vector vanishes identically and completely new phenomena occur where the equatorial region acts as a wave guide (Pedlosky 1979, Majda 2003). Other important phenomena in the tropical atmosphere are due to moist convection (Smith 1997), which supplies active mass sources and sinks to the fluid dynamics. Furthermore, all these effects combine to produce coherent multi-scale wave patterns that profoundly influence long-term mid-latitude weather prediction and climate change through hurricanes,

---

*Corresponding author. Email: jonjon@cims.nyu.edu

monsoons, El Niño, and global teleconnections (Mapes *et al.* 2006). Recently, in this context, new multi-scale balanced models have been developed (Sobel *et al.* 2001, Majda and Klein 2003, Klein and Majda 2006, Majda 2007a,b) and applied (Biello and Majda 2005, 2006, Biello *et al.* 2007) systematically to these problems. The two common assumptions in the development of these multi-scale models is the horizontal weak temperature gradient (WTG) approximation for potential temperature

$$\Theta = \overline{\Theta}(z) + \epsilon\theta(\mathbf{x}_h, z, t), \quad \epsilon \ll 1, \tag{1}$$

and the low Froude number approximation for the horizontal flow $\mathbf{U}_h$

$$\mathbf{U}_h = \epsilon\mathbf{u}_h, \quad \epsilon \ll 1. \tag{2}$$

In (2), $\mathbf{u}_h = (u, v)$ is the horizontal velocity and $\epsilon = \mathrm{FR}$, the Froude given by $\mathrm{FR} = |\mathbf{u}_h|/(NH)$, with N the buoyancy frequency associated with $\overline{\Theta}(z)$ (Majda 2003). Values of ϵ in the range $\epsilon \cong 1/10$ to $1/7$ are typical observed values for the lower/middle troposphere in the tropical atmosphere and simplified multi-scale balanced models arise on horizontal scales ranging from microscales of order 10 km to planetary scales of order 10,000 km (Klein 2000, Majda and Klein 2003, Biello and Majda 2006, Klein and Majda 2006, Majda 2007a,b); the basis for utilizing the WTG assumption in (1) is the observed small horizontal fluctuations of temperature in the tropics.

With the above background, the goal here is to study a canonical balanced model, which arises systematically in the above context (on various spatio-temporal scales). This model is given by **vertically sheared horizontal flow with mass (heat) sources (VSHFS)** and has the canonical form

$$\begin{aligned}
\frac{\mathrm{D}\mathbf{u}_h}{\mathrm{D}t} + fu_h^\perp &= -\nabla_h p + \mathbf{S_u}, \\
\nabla_h \cdot \mathbf{u}_h + w_z &= 0, \\
wN^2(z) &= S_\theta,
\end{aligned} \tag{3}$$

where $N(z)$ is the buoyancy frequency and S_θ and $\mathbf{S_u}$ are mass (heat) and momentum sources, respectively. In (3), $(\mathbf{u}_h^\perp, w)^t$ is the total velocity with $\mathrm{D}/\mathrm{D}t = \partial/\partial t + \mathbf{u}_h \cdot \nabla_h + w\partial/\partial z$, $\mathbf{u}_h^\perp = (-v, u)^t$, f, a constant nondimensional vertical rotation component and $\nabla_h\cdot, \nabla_h$, the horizontal divergence and gradient. Actually, an anelastic version of (3) arises in applications but a simple density coordinate reduces the equations to the form in (3).

The equations in (3) arise in a variety of multiple spatial scale balanced dynamics for the tropics: on horizontal scales of order 1500 km and time scales of order 8 h (see the BMESD model in Majda 2007b); on horizontal scales of order 10 km and time scales of order 15 min (Klein 2000, Klein and Majda 2006); with the beta plane approximation, $f = \beta y$, on horizontal scales of order 800 km and time scales on the order of 1 day (Sobel *et al.* 2001, Majda and Klein 2003); even on seasonal planetary scales (see, SPEWTG model in Majda and Klein 2006). There is a wide current interest in the outstanding problem of hurricane formation and the nature of the preconditioning environment, which leads to cyclogenesis, the hurricane embryo (Hendricks *et al.* 2004, Montgomery *et al.* 2006). In section 2 below, we present a brief sketch of the fashion in which the canonical model in (3), arises on two different spatio-temporal scales as models of interest for the hurricane embryo.

The remainder of this article is devoted to the analytic properties of solutions of (3) with the emphasis on the new phenomena produced by a nonzero vertical velocity w. In section 3, general systematic exact solutions of (3), which are linear flow fields in the spatial coordinates are introduced as background flows (Craik and Criminale 1986, Majda 2003); these solutions are regarded as elementary local large-scale preconditioning fields; exact nonlinear plane wave solutions for vertical vorticity are developed, which address their instability following a route pioneered by Craik and Criminale (1986) (also see Craik 1989, Lifschitz and Hameiri 1991, Craik and Allen 1992, Bayly *et al.* 1996, Majda and Shefter 1998, Majda 2003). In section 4, motivated by the role of (3) for the hurricane embryo, we study radial eddy "hot towers" for (3) in various radial preconditioning environments through elementary exact solution formulas and numerics.

Finally, we note that the balanced dynamic equations in (3) with $S_\theta \equiv 0$, $w \equiv 0$ involving purely horizontal flow arise as a canonical balanced model for strongly stratified flow (Embid and Majda 1998, Riley and Lelong 2000); these balanced dynamics have already been useful as models for laboratory experiments in decaying stratified flow (Majda and Grote 1993, Fincham *et al.* 1996, Majda 2003) and for explaining features of turbulent cascade in numerical experiments for strongly stratified flow (Smith 2001, Smith and Waleffe 2002, Waite and Bartello 2004). Here, the emphasis is on the new phenomena in (3), with a nonzero mass source, S_θ and vertical velocity w.

2. The canonical balanced model

First, we briefly sketch a self-contained derivation for the canonical model in (3) under natural hypotheses. This context is useful as a model for the hurricane embryo as noted in the introduction. Then, we study the general structure of the vorticity dynamics of (3). For simplicity in explanation, we start with the Boussinesq equation and follow the nondimensionalization in chapter 6 of Majda (2003). Thus, we assume an isotropic scale $H = L$, with Froude number $\mathrm{FR} = U/(NL) = \epsilon$, comparable horizontal and vertical velocity magnitudes, Rossby number $\mathrm{RO} = V/(Lf) \gg O(1)$, the Euler number $\sim O(1)$ and consistent with the WTG approximation in (1),

$$\Theta = z + \epsilon\theta, \quad \epsilon \ll 1. \tag{4}$$

If the unit of time is given by the advection time-scale $T = L/V$, with all these assumptions, the forced Boussinesq equations can be written in the nondimensional form

$$\begin{aligned}
\frac{\mathrm{D}\mathbf{u}_h}{\mathrm{D}t} + (\mathrm{Ro})^{-1}\mathbf{u}_h^\perp &= -\nabla_h p + \mathbf{S_u}, \\
\frac{\mathrm{D}w}{\mathrm{D}t} &= -\frac{\partial p}{\partial z} + \epsilon^{-1}\theta + S_w, \\
\frac{\mathrm{D}\theta}{\mathrm{D}t} &= \epsilon^{-1}(-w + S_\theta), \\
\nabla_h \cdot \mathbf{u}_h + w_z &= 0.
\end{aligned} \tag{5}$$

Note that the heat source term S_θ has been given the magnitude ϵ^{-1} in the potential temperature equation in (5); in other words, from (4) the magnitude of heating is strong

with the order $|\Theta|/T$ in nondimensional units. The formal derivation of the canonical model (3) is straightforward, since these are just the leading-order ϵ^0 equations for horizontal momentum, and mass conservation and the leading-order ϵ^{-1} equations for the potential temperature. If the temperature perturbation θ is expanded as $\theta = \epsilon\theta_1$, then θ_1 is determined diagnostically from the solution of (3) as given by

$$\theta_1 = \frac{\mathrm{D}w}{\mathrm{D}t} + \frac{\partial p}{\partial z} - S_w. \tag{6}$$

This completes the derivation. Note that $(\mathrm{Ro})^{-1}$ in (5) has been identified with f in (3).

The above model regime for (3) has direct relevance for the troposphere with $N^2 \cong 10^{-4}\,\mathrm{s}^{-1}$ with the scales $L = H = 10\,\mathrm{km}$, $|\mathbf{u}| = |w| = 10\,\mathrm{m\,s}^{-1}$, $T = 15\,\mathrm{min}$, $[\Theta] = 30°\,\mathrm{K}$, and

$$\mathrm{Ro} = \epsilon^{-1}(\sin\phi_0)^{-1}, \tag{7}$$

with ϕ_0 a given latitude (Klein 2000, Klein and Majda 2006, Majda 2007a). Thus, the strong heating rate for applicability of the canonical equations in (3) in the present setting is $30°\,\mathrm{K}/15\,\mathrm{min}$ or $120°\,\mathrm{K\,h}^{-1}$; this is the approximate magnitude of the heating rate observed in the "hot towers", which occur on scales of order $10\,\mathrm{km}$ through moist deep convection in the hurricane embryo (Hendricks *et al.* 2004, Montgomery *et al.* 2006). Thus, the models in (3) without rotation should be useful for studying the balanced dynamic response for hot towers. Elementary models for this behavior are discussed in section 4 below.

The canonical models in (3) also apply on horizontal scales of order $100\,\mathrm{km}$ and timescales of order $2.5\,\mathrm{h}$; these timescales are relevant for the formation of mesovortices in the hurricane embryo (Montgomery *et al.* 2006). To establish this fact, introduce the aspect ratio $A = H/L$, $A \leq 1$ and the new rescaled variables

$$
\begin{aligned}
T = At, \quad X = Ax_h, \quad w = Aw_A, \\
(\mathrm{Ro})_A = A\mathrm{Ro}, \quad AS_{\theta,A} = S_\theta, \quad A\mathbf{S}_{\mathbf{u},A} = \mathbf{S}_{\mathbf{u}}.
\end{aligned}
\tag{8}
$$

With these rescaling, the equations in (5) become

$$
\begin{aligned}
\frac{\mathrm{D}\mathbf{u}_h}{\mathrm{D}T} + (\mathrm{Ro})_A^{-1}\mathbf{u}_h^\perp &= -\nabla_h p + \mathbf{S}_{\mathbf{u},A}, \\
A^2 \frac{\mathrm{D}w_A}{\mathrm{D}T} &= -\frac{\partial p}{\partial z} + \epsilon^{-1}\theta + S_w, \\
\frac{\mathrm{D}\theta}{\mathrm{D}T} &= \epsilon^{-1}(-w_A + S_{\theta,A}), \\
\nabla_X \cdot \mathbf{u}_h + (w_A)_z &= 0.
\end{aligned}
\tag{9}
$$

The derivation given below (5) can be repeated now for any A with $A \ll 1$ to yield (3) as a canonical balanced model provided that $(\mathrm{Ro})_A^{-1}$ remains finite. For the atmosphere where (7) is satisfied, the natural choice is $A = \epsilon$ yielding the canonical balanced dynamics in (3) on horizontal length scales of order $100\,\mathrm{km}$ on time-scales of order $2.5\,\mathrm{h}$ with heat sources of allowed strength $1°\,\mathrm{K\,h}^{-1}$, horizontal winds of order $10\,\mathrm{ms}^{-1}$, and nonzero order one effect of rotation for (3) with

$$f = \sin\phi_0. \tag{10}$$

The only difference is the equation for θ_1 in (6) does not have $\mathrm{D}w/\mathrm{D}t$. Systematic multi-scale models of this type for the hurricane embryo are developed elsewhere (Majda *et al.* 2008).

2.1. *Vertical vorticity dynamics*

To understand the dynamics contained in the balanced model in (3), it is useful to utilize the horizontal Helmholtz decomposition

$$\mathbf{u}_h = \nabla_h \Phi + \nabla_h^\perp \Psi + \mathbf{b}(z, t), \tag{11}$$

where Ψ is the stream function, Φ is the velocity potential, and $\mathbf{b}(z, t)$ is the specified background shear. From (3), we have that Φ is determined from the source S_θ by

$$\triangle_h \Phi = -w_z, \quad w = S_\theta. \tag{12}$$

Consistent with our discussion, here we assume constant $N^2(z)$. The equation for the stream function is given through the dynamics of the vertical vorticity

$$\omega = \triangle_h \Psi. \tag{13}$$

While it is not difficult to take the curl of (3) to obtain a dynamic equation for ω, it is illustrative to utilize Ertel's potential vorticity equation directly for (5) to derive this vortex dynamics (Embid and Majda 1998, Majda 2003).

The potential vorticity is defined by $q = (\omega + \mathrm{Ro}^{-1}\mathbf{e}_3) \cdot \nabla\Theta$, with $\omega = \nabla \times \mathbf{v}$. With the sources S_θ, and $\mathbf{S_v} = (\mathbf{S_u}, S_w)$, Ertel's theorem (Majda 2003) for (5) becomes

$$\frac{\mathrm{D}q}{\mathrm{D}t} = (\omega + \mathrm{Ro}^{-1}\mathbf{e}_3) \cdot \nabla S_\theta + (\nabla \times \mathbf{S_v}) \cdot \nabla\Theta. \tag{14}$$

To compute $\omega = \nabla \times \mathbf{v}$, it is convenient to write $\mathbf{v} = (\mathbf{u}_h, 0)^t + (\mathbf{0}, w)^t$ and calculate

$$\nabla \times \begin{pmatrix} \mathbf{u}_h \\ 0 \end{pmatrix} = \begin{pmatrix} \dfrac{\partial \mathbf{u}_h^\perp}{\partial z} \\ \omega \end{pmatrix},$$
$$\nabla \times \begin{pmatrix} \mathbf{0} \\ w \end{pmatrix} = \begin{pmatrix} -\nabla_h^\perp w \\ 0 \end{pmatrix}. \tag{15}$$

With (4) and (5), to leading-order $q = \omega + \mathrm{O}(\epsilon)$, $w = S_\theta + \mathrm{O}(\epsilon)$, so that (14) and (15) with $f = \mathrm{Ro}^{-1}$ yield the leading-order **vertical vorticity dynamic equation**

$$\frac{\mathrm{D}\omega}{\mathrm{D}t} = (\omega + f)(S_\theta)_z + \left(\frac{\partial}{\partial z}\mathbf{u}_h^\perp\right) \cdot \nabla_h S_\theta + \nabla_h \times \mathbf{S_u}. \tag{16}$$

The equations in (11–13), and (16) are the vorticity dynamic form of the balanced model in (3) with $N^2 = 1$. Alternatively, the reader can take the curl of the momentum equation in (3) directly and obtain (16).

The vorticity production term in the vertical vorticity dynamic equation (16) is decomposed, using the Helmholtz decomposition (11), as

$$\frac{\partial \mathbf{u}_h^\perp}{\partial z} \cdot \nabla_h w = -\left(\nabla_h^\perp w \cdot \frac{\partial \mathbf{b}}{\partial z}\right) - \left(\nabla_h^\perp w \cdot \frac{\partial \nabla_h \Phi}{\partial z}\right) - \left(\nabla_h^\perp w \cdot \frac{\partial \nabla_h^\perp \Psi}{\partial z}\right), \tag{17}$$

where the first term is the heating/background shear production source, the second term represents the heating generated shear production source, and the last term arises from heating and active shear. Hence, dynamic equation for vorticity (16) becomes

$$\frac{D\omega}{Dt} = (\omega + f)w_z - \nabla_h^{\perp} w \cdot \frac{\partial \mathbf{b}}{\partial z} - \nabla_h^{\perp} w \cdot \frac{\partial \nabla_h \Phi}{\partial z} - \nabla_h^{\perp} w \cdot \frac{\partial \nabla_h^{\perp} \Psi}{\partial z} + \nabla_h \times \mathbf{S_u}. \tag{18}$$

3. Exact solutions and their nonlinear stability

In this section, we first present general exact flow fields of the dynamic equation (3) given by velocity fields that are linear in the spatial coordinates. Taking them as local large-scale preconditioning fields, we then establish a general set-up for the stability analysis of the nonlinear plane wave perturbation of vertical vorticity. Stability in various cases based on varying the given linear heating source is then explored by a combination of theoretical exact solutions and elementary numerics. Here $\mathbf{S_u}$ is ignored to simplify the presentation.

3.1. *The reduced system for a linear heat source*

For linear flow fields, we consider the vertical velocity w specified by

$$w = S_\theta = \mathbf{l} \cdot \mathbf{x}_h + \alpha z, \tag{19}$$

with $\mathbf{l} = (l_1(t),\ l_2(t))^T$ and $\alpha = \alpha(t)$. It has a nice physical interpretation as explained below. To have a clear idea about the effect of α, we consider a simple case with $\mathbf{l} = (l, 0)$, and graph w at three different cases when $\alpha > 0$, $\alpha < 0$, and $\alpha = 0$. The results are shown in figure 1. As given in the figure 1(a), $\alpha > 0$ represents the structure with rising air ($w > 0$) above and descending air ($w < 0$) below, i.e. heating above and cooling below; this phenomenon is called a stratiform type cloud in the meteorology (Ackerman and Knox 2003). As shown in the figure 1(b), $\alpha < 0$ means rising air below and descending air above, i.e. cooling above and heating below; this corresponds to a congestus-type cloud in the meteorology. The figure 1(c) shows the situation when $\alpha = 0$, where the heating has no vertical dependence. A transition between descending air in the left plane and rising air in the right-half plane can be observed.

Under the linear heating condition (19), together with the equation for the stream function (13), the vorticity equation in (18) takes the following form

$$\frac{\partial \omega}{\partial t} + J(\Psi, \omega) + \mathbf{b}(z, t) \cdot \nabla_h \omega - \frac{\alpha}{2} \mathbf{x}_h \cdot \nabla_h \omega$$

$$+ (\mathbf{l} \cdot \mathbf{x}_h + \alpha z) \frac{\partial \omega}{\partial z} - \alpha(\omega + f) + \mathbf{l}^{\perp} \cdot \frac{\partial}{\partial z} \nabla_h^{\perp} \Psi + \mathbf{l}^{\perp} \cdot \frac{\partial}{\partial z} \mathbf{b}(z, t) = 0 \tag{20a}$$

$$\triangle_h \Psi = \omega, \tag{20b}$$

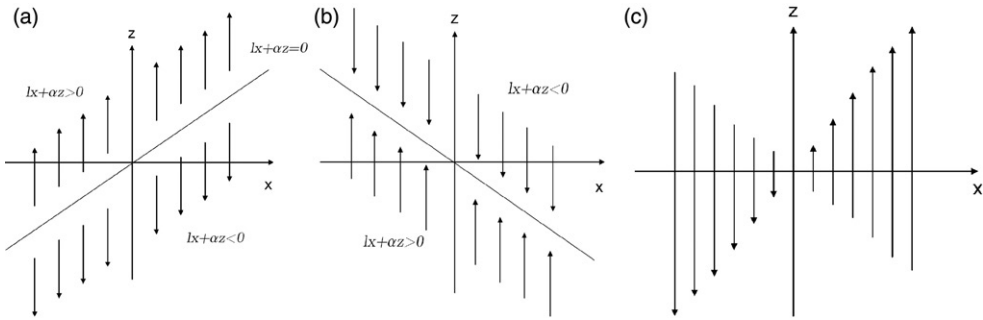where $J(\Psi(\mathbf{x}, t), \omega(\mathbf{x}, t)) = \nabla_h^{\perp} \Psi \cdot \nabla_h \omega$.

Figure 1. The structure of vertical velocity *w* in 2D environment; (a): Stratiform-type cloud when $\alpha > 0$, $l < 0$; (b): Congestus-type cloud when $\alpha < 0$, $l < 0$; (c): Structure when $\alpha = 0$, $l < 0$.
Note: Note the arrows are not representative of magnitude.

3.2. *Exact large-scale linear flows*

We begin with exact large-scale linear flow solutions.

PROPOSITION 1   *For the vertically sheared horizontal flow with heat source*

$$\frac{D}{Dt}\mathbf{u_h} + f\mathbf{u_h}^{\perp} = -\nabla_h p,$$

$$\nabla_h \cdot \mathbf{u_h} + w_z = 0,$$

$$w = S_\theta,$$

with f, a fixed constant representing the Coriolis effect and S_θ a linear function of $\mathbf{x}$, *z*,
there are exact linear solutions of the form

$$w = S_\theta = \mathbf{l} \cdot \mathbf{x}_h + \alpha z, \tag{21a}$$

$$\bar{\mathbf{u}}_h = -\frac{\alpha}{2}\mathbf{x}_h + \frac{1}{2}\bar{\omega}(t)\mathbf{x}_h^{\perp} + \mathcal{D}_h(t)\mathbf{x}_h + \mathbf{b}z, \tag{21b}$$

where $\mathcal{D}_h$ is an arbitrary 2×2, traceless, symmetric matrix, $\mathbf{b} = (b_1(t), b_2(t))^T$ is a vector describing the background shear and $\bar{\omega}(t) = \nabla_h \times \bar{\mathbf{u}}_h$ satisfies

$$\frac{\partial \overline{\omega}}{\partial t} = \alpha(\overline{\omega} + f) - \mathbf{l}^{\perp} \cdot \mathbf{b}, \quad \overline{\omega}(0) = \overline{\omega}_0. \tag{22}$$

The proof of proposition 1 follows the techniques presented in chapter 2 of Majda (2003). We refer to appendix A for details, and also formulas for the pressure.
The linear vorticity equation (22) leads to

$$\overline{\omega}(t) = e^{\int_0^t \alpha ds}\left(\overline{\omega}_0 + \int_0^t (\alpha f - \mathbf{l}^{\perp} \cdot \mathbf{b})e^{-\int_0^s \alpha ds'}\, ds\right). \tag{23}$$

To simplify our discussion below, we assume α is a constant and $\mathbf{l}^{\perp} \cdot \mathbf{b}$ is independent of *t*, which lead to

$$\overline{\omega}(t) = \begin{cases} e^{\alpha t}\left(\overline{\omega}_0 + f - \dfrac{1}{\alpha}\mathbf{l}^{\perp} \cdot \mathbf{b}\right) - f + \dfrac{1}{\alpha}\mathbf{l}^{\perp} \cdot \mathbf{b} & \text{if} \quad \alpha \neq 0, \\ \\ \overline{\omega}_0 - (\mathbf{l}^{\perp} \cdot \mathbf{b})t & \text{if} \quad \alpha = 0. \end{cases} \tag{24}$$

Note that $\overline{\omega} > 0$ means cyclones in northern hemisphere (anti-clockwise vortices), and $\overline{\omega} < 0$ means anti-cyclones (clockwise vortices). In the vorticity equation (22), $\alpha\overline{\omega}$ is the stretching term and $\mathbf{l}^{\perp} \cdot \mathbf{b}$, αf are both source terms, which determine whether cyclones or anti-cyclones are created. We consider different cases below.

- $\alpha > 0$, where the rising air is above the descending air and a stratiform-type cloud is generated.

  In this case, growing vorticity occurs. The competition between the effects of background flow and the Coriolis effect determines whether cyclones or anti-cyclones are created by the sign of the forcing term $\overline{\omega}_0 + f - 1/\alpha \mathbf{l}^{\perp} \cdot \mathbf{b}$.

- $\alpha < 0$, where the rising air is below the descending air and a congestus-type cloud is generated.

  In this case, a steady limiting flow is observed with

$$\overline{\omega} \to -f + \frac{1}{\alpha}\mathbf{l}^{\perp} \cdot \mathbf{b}. \tag{25}$$

  The flow swirls as cyclones or anti-cyclones, depending on the sign of the term $-f + 1/\alpha \, \mathbf{l}^{\perp} \cdot \mathbf{b}$.

- $\alpha = 0$, where heating has no vertical dependence.

  In this case, linearly growing vorticity occurs, with cyclones or anti-cyclones determined by the sign of $\mathbf{l}^{\perp} \cdot \mathbf{b}$.

In order to illustrate the flow generated by linear heating, we provide several instantaneous plots of velocity fields with no strain flow [i.e. $\mathcal{D}_h(t) = 0$ in (21b)]. The initial vorticity $\overline{\omega}_0$ is chosen as 0 to represent an environment with no vorticity. We start with the case $\alpha = 1$, and show the velocity fields at time $t = 3.5$. Four plots with different parameters $\mathbf{b}$ (background shear) and $\mathbf{l}$ (spatial tilting of vertical velocity) are given in figure 2; they show that modification of $\mathbf{l}$ when $\mathbf{b} = 0$ does not affect the horizontal field, and background shear only changes the center of the cyclone if $\mathbf{l} = 0$. We also observe that as $\mathbf{b}$ increases when $\mathbf{l}$ is fixed, the cyclones become weaker first [figure 2(c)], and then anti-cyclones are generated [figure 2(d)]. This is due to the fact that the forcing term $\overline{\omega}_0 + f - 1/\alpha \mathbf{l}^{\perp} \cdot \mathbf{b}$ decreases as $\mathbf{b}$ increases for this fixed $\mathbf{l}$. To show how this linear flow changes vertically, we present a 3D plot corresponding to the figure 2(d) above, with two slices of horizontal velocity fields, in figure 3. This shows that the center of anti-cyclones changes due to the effect of the background shear. In figure 4, we show streamlines spinning up through a fixed point, under two different sets of $\mathbf{l}$ and $\mathbf{b}$ corresponding to the figure 2(a) and (d), respectively, which also shows how the background shear changes the center of the vortex. Finally, we considered the case $\alpha = -1$ and similar behavior is observed (not shown).

3.3. *Nonlinear plane wave perturbation of the linear flow fields*

The exact linear flow field solutions (21), as discussed in the previous section, serve as local large-scale preconditioning fields. Here, we establish a general set-up for the stability analysis of the nonlinear plane wave perturbation of vertical vorticity. We are interested to know how the vorticity amplifies and along which directions it is unstable. For simplicity, the strain flow is ignored in the following discussion.
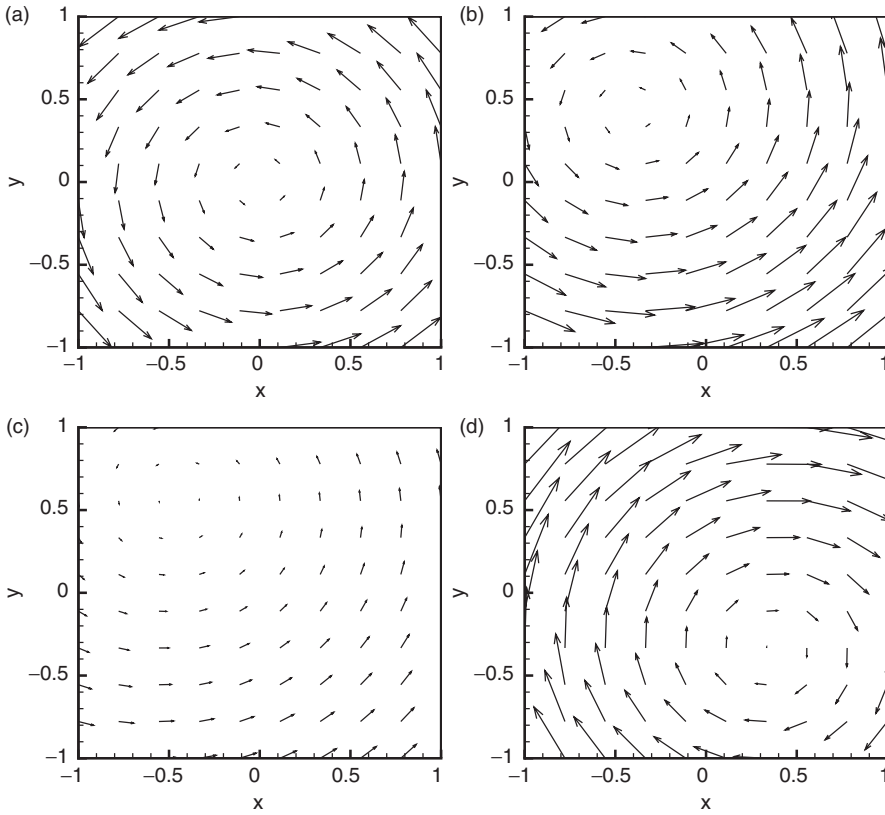
Figure 2. The vector field of the horizontal velocity under different parameters at $z = 1$, and $t = 3.5$ when $\alpha = 1$, $f = 1$, and $\bar{\omega}_0 = 0$; (a): arbitrary $\mathbf{l}$, $\mathbf{b} = 0$; (b): $\mathbf{l} = 0$, $\mathbf{b} = (6, 6)$; (c): $\mathbf{l} = (1/5, -1/6)$, $\mathbf{b} = (2, 2)$; (d): $\mathbf{l} = (1/5, -1/6)$, $\mathbf{b} = (6, 6)$.

We explore the nonlinear plane wave perturbation ω' about the large-scale linear flow (21, 22) of the form

$$\omega(\mathbf{x_h}, z, t) = \bar{\omega}(t) + \omega'(\mathbf{x_h}, z, t), \tag{26}$$

$$\Psi(\mathbf{x_h}, z, t) = \bar{\Psi}(\mathbf{x_h}, t) + \Psi'(\mathbf{x_h}, z, t) = \frac{\bar{\omega}(t)}{4}\mathbf{x_h} \cdot \mathbf{x_h} + \Psi'(\mathbf{x_h}, z, t). \tag{27}$$

Under this decomposition, the vorticity equation (20) leads to

$$\frac{\partial \omega'}{\partial t} + J(\Psi', \omega') + \left(\frac{\bar{\omega}(t)}{2}\mathbf{x_h^\perp} - \frac{\alpha}{2}\mathbf{x}_h + \mathbf{b}z\right) \cdot \nabla_h \omega' + (\mathbf{l} \cdot \mathbf{x}_h + \alpha z)\frac{\partial \omega'}{\partial z}$$

$$- \alpha\omega' + \mathbf{l}^\perp \cdot \frac{\partial}{\partial z}\nabla_h^\perp \Psi' = 0 \tag{28a}$$

$$\triangle_h \Psi' = \omega'. \tag{28b}$$

Hence, the velocity is given by

$$\mathbf{u}_h = \bar{\mathbf{u}}_h + \nabla_h^\perp \Psi', \tag{29}$$

where $\bar{\mathbf{u}}_h$ is the linear horizontal velocity defined in (21b) with $\mathcal{D}_h(t) = 0$. For convenience, we drop the prime in the following.
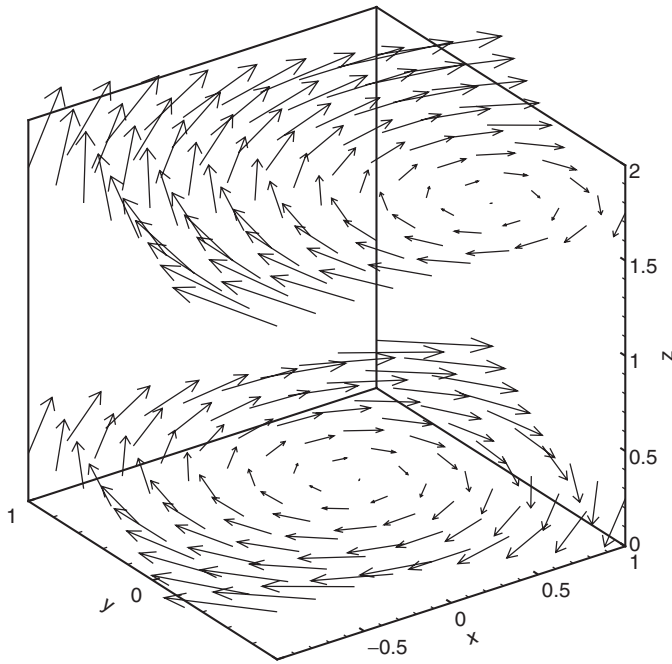
Figure 3.   Two vertical slices of horizontal velocity fields at $z = 0.25$ and $z = 1.75$, when $\alpha = 1$, $t = 3.5$, $f = 1$, $\bar{\omega}_0 = 0$, $\mathbf{l} = (1/5, -1/6)$, and $\mathbf{b} = (6,6)$.
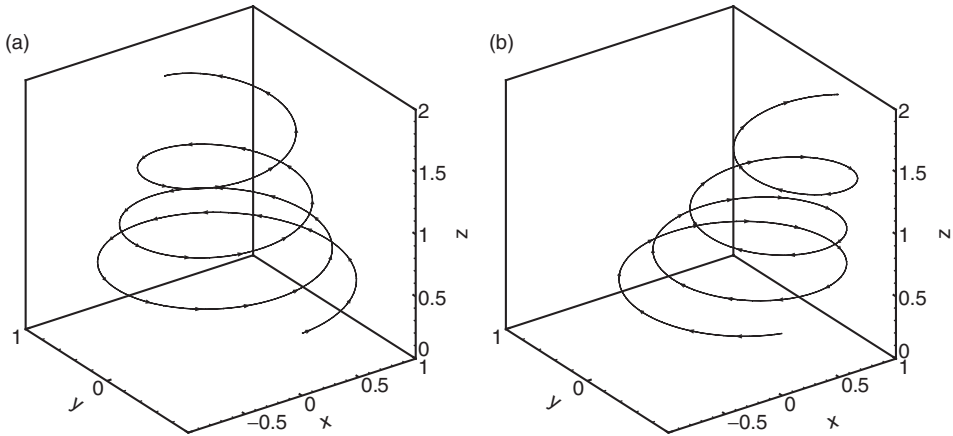
Figure 4.   A streamline spinning up through point $(0, -1, 0.5)$, when $t = 3.5$, $\alpha = 1$, $f = 1$, and $\bar{\omega}_0 = 0$; (a): anti-clockwise, with $\mathbf{l} = \mathbf{b} = 0$; (b): clockwise, with $\mathbf{l} = (1/5, -1/6)$, $\mathbf{b} = (6,6)$.

With the matrix

$$A(t) = \begin{bmatrix} -\dfrac{\alpha}{2} & -\dfrac{\bar{\omega}(t)}{2} & b_1 \\[2mm] \dfrac{\bar{\omega}(t)}{2} & -\dfrac{\alpha}{2} & b_2 \\[2mm] l_1 & l_2 & \alpha \end{bmatrix}, \tag{30}$$

the vorticity equation for perturbations in (28) is then given by

$$\frac{\partial \omega}{\partial t} + J(\Psi, \omega) + A(t)\mathbf{x} \cdot \nabla \omega - \alpha \omega + \mathbf{l}^{\perp} \cdot \frac{\partial}{\partial z} \nabla_h^{\perp} \Psi = 0, \tag{31a}$$

$$\Delta_h \Psi = \omega. \tag{31b}$$

In order to remove the advection term $A(t)\mathbf{x} \cdot \nabla \omega$ from this equation, we introduce characteristic coordinates $\xi = \xi(\mathbf{x}, t)$ with inverse $\mathbf{X} = \mathbf{X}(\xi, t)$ following the technique presented in chapter 3 of Majda (2003), so that

$$\frac{\mathrm{d}}{\mathrm{d}t} \mathbf{X}(\xi, t) = A(t)\mathbf{X}(\xi, t), \quad \mathbf{X}(\xi, 0) = \xi. \tag{32}$$

The vorticity-stream formulation in the new characteristic coordinates ξ is given by

$$\frac{\partial}{\partial t} \omega(\xi, t) - \alpha \omega(\xi, t) + J(\Psi(\mathbf{x}, t), \omega(\mathbf{x}, t)) + \mathbf{l}^{\perp} \cdot \frac{\partial}{\partial z} \nabla_h^{\perp} \Psi = 0 \tag{33a}$$

$$\Delta_h \Psi = \omega, \tag{33b}$$

where $\triangle_h$ and ∇_h are the operators in the Eulerian coordinates $\mathbf{x}$. Here we keep a mixture of $\mathbf{x}$ and ξ for notation convenience, although we eventually switch completely to ξ coordinates. The coordinate transformation in (32) is given by

$$\mathbf{X} = \mathrm{e}^{\int_0^t A(s)\mathrm{d}s} \xi, \tag{34}$$

where $\mathrm{e}^{\int_0^t A(s)\mathrm{d}s}$ is a time-ordered exponential representing the fundamental solution matrix of (32). To analyze (33), we set

$$\omega = \widehat{\omega}_{\mathbf{k}}(t)\mathrm{e}^{\mathbf{i}\mathbf{k}\cdot\xi} = \widehat{\omega}_{\mathbf{k}}(t)\mathrm{e}^{\mathbf{i}(k_1\xi_1 + k_2\xi_2 + k_3\xi_3)}. \tag{35}$$

In appendix B, we show the following formula for the amplitude $\widehat{\omega}_{\mathbf{k}}(t)$

$$\frac{\mathrm{d}}{\mathrm{d}t} \widehat{\omega}_{\mathbf{k}}(t) = (\alpha - S(t, \mathbf{k}))\widehat{\omega}_{\mathbf{k}}(t), \tag{36}$$

with

$$S(t, \mathbf{k}) = \frac{\sum_{i,j=1}^3 \left(l_1 \frac{\partial \xi_i}{\partial z} \frac{\partial \xi_j}{\partial x} + l_2 \frac{\partial \xi_i}{\partial z} \frac{\partial \xi_j}{\partial y} \right) k_i k_j}{\sum_{i,j=1}^3 \left(\frac{\partial \xi_i}{\partial x} \frac{\partial \xi_j}{\partial x} + \frac{\partial \xi_i}{\partial y} \frac{\partial \xi_j}{\partial y} \right) k_i k_j}, \tag{37}$$

where each derivative term, for example, $\partial \xi_i / \partial x$, is an element of the ordered exponential $(\mathrm{e}^{\int_0^t A(s)\mathrm{d}s})^T$ in (B.1).

We have thus shown the following:

PROPOSITION 2 *For given linear heat source (19), the system (3) has exact solutions of the form*

$$\omega(\mathbf{x_h}, z, t) = \bar{\omega}(t) + \omega'(\mathbf{x_h}, z, t),$$

where $\bar{\omega}$ is given in (22) and $\omega' = \widehat{\omega}_{\mathbf{k}}(t)\mathrm{e}^{\mathbf{i}\mathbf{k}\cdot\xi}$, with the characteristic coordinates ξ defined in (34) and the amplitude $\widehat{\omega}_{\mathbf{k}}$ determined by (36) as a nonlinear solution of the vorticity-stream formulation in (33).

3.4. *Amplification of vertical vorticity in background linear flow fields*

In the previous section, we presented a strategy to analyze plane wave perturbations through the simplified system (36). Here we study the stability of the perturbation flow in various cases, to illustrate how the vorticity grows and when it stays stable. Analysis is based on a combination of exact solutions and elementary numerics, for different cases determined by the parameters α, $\mathbf{l}$ (describing the heat source), and $\mathbf{b}$ (describing background shear). The results are summarized below, and explained in more detail in the following parts. For simplicity, we assume all the parameters α, $\mathbf{l}$, and $\mathbf{b}$ are constant, and $\overline{\omega}_0$ is zero.

3.4.1. Summary

- *Case 1* No heat source, and nonzero background shear ($\alpha = 0$, $\mathbf{l} = 0$, and $\mathbf{b} \neq 0$). This is the barotropic situation, and the plane wave perturbation is stable for all wave numbers.
- *Case 2* Heat source with no horizontal dependence ($\alpha \neq 0$ and $\mathbf{l} = 0$). The results, shown in table 1, are obtained by theoretical analysis.
- *Case 3* Heat source with no vertical dependence ($\alpha = 0$ and $\mathbf{l} \neq 0$).
  We denote $D = \mathbf{l} \cdot \mathbf{b} = \nabla_h w \cdot \mathbf{b}$, the directional derivative of vertical velocity w along the background shear direction $\mathbf{b}$. It represents the coupling of background shear and spatial tilt of heating.
  The results are shown in table 2, where the regime $b = 0$ is analyzed based on theoretical exact solutions and the other regime is analyzed based on elementary numerics.
- *Case 4* Heat source with both horizontal and vertical dependence and no background shear ($\alpha \neq 0$, $\mathbf{l} \neq 0$, and $\mathbf{b} = 0$).
  The results are shown in table 3. When $\overline{\omega}(t) = 0$, an exact solution of (36) can be derived, and stability can then be analyzed theoretically. The other regime

Table 1. Stability of the amplitude $\hat{\omega}_{\mathbf{k}}(t)$ when $\alpha \neq 0$ and $\mathbf{l} = 0$.

$\alpha > 0$	$\alpha < 0$
Unstable with exponential growth $e^{\alpha t}$ for all wave numbers.	Stable with exponential decreasing rate $e^{\alpha t}$ for all wave numbers.

Table 2. Stability of the amplitude $\hat{\omega}_{\mathbf{k}}(t)$ when $\alpha = 0$ and $\mathbf{l} \neq 0$.

| | $b = 0$ | $b \neq 0$ | |
		$D > 0$	$D < 0$
$\bar{\omega} = 0$		Unstable with exponential growth $e^{\sqrt{D}t}$ for all wave numbers.	Stable with bounded oscillating amplitude for all wave numbers.
$\bar{\omega} \neq 0$	Unstable with linear growth for all wave numbers except $k_3 = 0$.	Unstable with exponential growth for all wave numbers.	

$\overline{\omega}(t) \neq 0$ is studied based on elementary numerics. The results in table 3 are interesting since we already concluded in case 2 that the wave is stable for $\alpha < 0$ when $\mathbf{l} = 0$. Here, we show that *a slight tilting of the heating will lead to instability* except along $k_3 = 0$.

- *Case 5* Heat source with both horizontal and vertical dependence and nonzero background shear ($\alpha \neq 0$, $\mathbf{l} \neq 0$, and $\mathbf{b} \neq 0$).

  This most general case, shown in table 4, is studied numerically. Depending on different parameters α, $\mathbf{b}$, and $\mathbf{l}$, different behavior of the amplitude $\widehat{\omega}_{\mathbf{k}}(t)$ can be obtained. Hence, compared to case 4, we show that *shear can stabilize the flow* in some cases when $\alpha < 0$ and two regimes are identified where the vertical velocity gradient α has a different stabilizing/destabilizing effects.

3.4.2. Case 1: No heat source, and nonzero background shear. We start with the barotropic case when there is no heat source. Hence, the background linear solution $\overline{\omega}(t)$ (24) equals $\overline{\omega}_0$, which is assumed to be zero here. In this case, the vorticity equation (31a) takes the form

$$\frac{\partial \omega}{\partial t} + J(\Psi, \omega) + A(t)\mathbf{x} \cdot \nabla \omega = 0, \tag{38}$$

where

$$A(t) = \begin{bmatrix} 0 & 0 & b_1 \\ 0 & 0 & b_2 \\ 0 & 0 & 0 \end{bmatrix}. \tag{39}$$

The vorticity stream formulation (33a) in the characteristic coordinates ξ becomes

$$\frac{\partial}{\partial t}\omega(\xi, t) + J(\Psi(\mathbf{x}, t), \omega(\mathbf{x}, t)) = 0, \tag{40}$$

Table 3. Stability of the amplitude $\hat{\omega}_{\mathbf{k}}(t)$ when $\alpha \neq 0$, $\mathbf{l} \neq 0$, and $\mathbf{b} = 0$.

	$\alpha > 0$	$\alpha < 0$
$\bar{\omega} = 0$	Unstable with exponential growth $e^{\alpha t}$ for all wave numbers except $\mathbf{k} = (2l_1, 2l_2, 3\alpha)$.	Unstable with exponential growth $e^{-\alpha t/2}$ for all wave numbers except $k_3 = 0$.
$\bar{\omega} \neq 0$	Unstable with exponential growth $e^{\alpha t}$ for all wave numbers.	Unstable with exponential growth $e^{-\alpha t/2}$ for all wave numbers except $k_3 = 0$.

Table 4. Stability of the amplitude $\hat{\omega}_{\mathbf{k}}(t)$ when $\alpha \neq 0$, $\mathbf{l} \neq 0$, and $\mathbf{b} \neq 0$.

$\alpha > 0$	$\alpha < 0$
Unstable with exponential growth $e^{\alpha t}$ for all wave numbers.	All these situations can happen: Unstable with exponential growth; Unstable with linear growth; Stable with bounded amplitude; Stable with amplitude decaying to zero.

with the coordinate transformation in (32) given by

$$\mathbf{X} = e^{\int_0^t A(s)ds}\xi = \begin{bmatrix} 1 & 0 & b_1 t \\ 0 & 1 & b_2 t \\ 0 & 0 & 1 \end{bmatrix}\xi. \tag{41}$$

The equation for the amplitude $\widehat{\omega}_{\mathbf{k}}(t)$ in (36) becomes

$$\frac{\mathrm{d}}{\mathrm{d}t}\widehat{\omega}_{\mathbf{k}}(t) = 0 \Rightarrow \widehat{\omega}_{\mathbf{k}}(t) = \widehat{\omega}_{\mathbf{k}}(0). \tag{42}$$

Thus, we have the following:

PROPOSITION 3 *When there is no heating, vertical velocity is zero and the exact nonlinear plane wave perturbation solution of the vorticity-stream formulation (33) is stable and given by*

$$\omega(t) = \widehat{\omega}_{\mathbf{k}}(0)e^{i\mathbf{k}\cdot\xi} = \widehat{\omega}_{\mathbf{k}}(0)e^{i(\mathbf{k_h}\cdot\mathbf{x_h}+(k_3-\mathbf{k_h}\cdot\mathbf{b}t)z)}, \tag{43}$$

where $\mathbf{k_h} = (k_1, k_2)$.

3.4.3. Case 2: Heat source with no horizontal dependence.
First we study the case when $\mathbf{l} = 0$ and $\alpha \neq 0$, i.e. the heat source changes only in the vertical direction. When $\mathbf{b} = 0$, the perturbation is trivially stable if α is negative and unstable otherwise. Here we discuss the case $\mathbf{b} \neq 0$.

The vorticity equation (31a) takes the form

$$\frac{\partial\omega}{\partial t} + J(\Psi, \omega) + A(t)\mathbf{x}\cdot\nabla\omega - \alpha\omega = 0, \tag{44}$$

where

$$A(t) = \begin{bmatrix} -\dfrac{\alpha}{2} & -\dfrac{\bar{\omega}(t)}{2} & b_1 \\[2mm] \dfrac{\bar{\omega}(t)}{2} & -\dfrac{\alpha}{2} & b_2 \\[2mm] 0 & 0 & \alpha \end{bmatrix}. \tag{45}$$

The coordinate transformation in (32) is given by

$$\mathbf{X} = e^{\int_0^t A(s)ds}\xi = \begin{bmatrix} e^{-(\alpha t/2)}\cos(\bar{\theta}(t)) & -e^{-(\alpha t/2)}\sin(\bar{\theta}(t)) & a_{13}(t) \\ e^{-(\alpha t/2)}\sin(\bar{\theta}(t)) & e^{-(\alpha t/2)}\cos(\bar{\theta}(t)) & a_{23}(t) \\ 0 & 0 & e^{\alpha t} \end{bmatrix}\xi, \tag{46}$$

where $a_{13}(t)$ and $a_{23}(t)$ are defined as

$$a_{13}(t) = \frac{2te^{-(\alpha t/2)}\big(e^{(3\alpha t/2)}(3b_1\alpha t - b_2\bar{\theta}(t)) + \cos(\bar{\theta}(t))(-3b_1\alpha t + b_2\bar{\theta}(t)) + \sin(\bar{\theta}(t))(3b_2\alpha t + b_1\bar{\theta}(t))\big)}{9\alpha^2 t^2 + \bar{\theta}^2(t)},$$

$$a_{23}(t) = \frac{2te^{-(\alpha t/2)}\big(e^{(3\alpha t/2)}(3b_2\alpha t + b_1\bar{\theta}(t)) - \cos(\bar{\theta}(t))(3b_2\alpha t + b_1\bar{\theta}(t)) + \sin(\bar{\theta}(t))(-3b_1\alpha t + b_2\bar{\theta}(t))\big)}{9\alpha^2 t^2 + \bar{\theta}^2(t)},$$

and

$$\frac{\mathrm{d}}{\mathrm{d}t}\bar{\theta}(t) = \frac{\bar{\omega}(t)}{2}, \quad \bar{\theta}(0) = 0.$$

Then, the vorticity-stream formulation (33a) in the new characteristic coordinates ξ become

$$\frac{\partial}{\partial t}\omega(\xi, t) - \alpha\omega(\xi, t) + J(\Psi(\mathbf{x}, t), \omega(\mathbf{x}, t)) = 0. \tag{47}$$

Since $\mathbf{l} = 0$, $S(t, \mathbf{k})$ in (37) is zero, hence the amplitude $\widehat{\omega}_{\mathbf{k}}(t)$, computed in (36), is determined by the following equation

$$\frac{\mathrm{d}}{\mathrm{d}t}\widehat{\omega}_{\mathbf{k}}(t) = \alpha\widehat{\omega}_{\mathbf{k}}(t), \quad \widehat{\omega}_{\mathbf{k}}(t) = \mathrm{e}^{\alpha t}\widehat{\omega}_{\mathbf{k}}(0). \tag{48}$$

Thus, we have the following:

PROPOSITION 4 *If the linear vertical velocity is given by $w = \alpha z$, the exact nonlinear plane wave perturbation solution of the vorticity-stream formulation (33) is given by*

$$\omega = \widehat{\omega}_{\mathbf{k}}(t)\mathrm{e}^{\mathrm{i}\mathbf{k}\cdot\xi} = \mathrm{e}^{\alpha t}\widehat{\omega}_{\mathbf{k}}(0)\mathrm{e}^{\mathrm{i}\mathbf{k}\cdot\xi}, \tag{49}$$

where the characteristic coordinates ξ are defined in (46).

Note that the background shear flow $\mathbf{b}z$ only affects the direction of wave propagation through the coordinates ξ, and has no impact on the stability of the perturbation wave. As explained below, stability of the plane wave solution totally depends on the sign of α.

- $\alpha > 0$ (rising air above, generating a stratiform-type cloud)
    This case will have an exponentially growing solution of the form $\mathrm{e}^{\alpha t}$. We conclude that the plane wave perturbation is unstable.
- $\alpha < 0$ (descending air above, generating a congestus-type cloud)
    The plane wave perturbation decays to zero, and becomes negligible. The vorticity is dominated by the large-scale background vorticity in (24) and is independent of $\mathbf{x}$ as t approaches infinity.
- $\alpha = 0$ (no heat source)
    The amplitude of the plane wave perturbation remains constant, hence, the vorticity is dominated by the linearly growing large-scale preconditioned vorticity in (24).

Remark The plane wave propagates along the wave direction $\mathbf{k}$ in the characteristic coordinates ξ, defined in (46). We remark that a straight line in the ξ coordinates is no longer a line, but rather a complicated path in the $\mathbf{x}$ coordinates. For example, from (46), we know that a fixed point $\mathbf{k} = (1, 0, 0)$, represents $(\mathrm{e}^{-\alpha t/2}\cos(\bar{\theta}(t)), \mathrm{e}^{-\alpha t/2}\sin(\bar{\theta}(t)), 0)$ at different time t in the $\mathbf{x}$ coordinates. Its trajectory is a helix for negative α.

3.4.4. Case 3: Heat source with no vertical dependence.
Here we consider the case when $w = S_\theta = \mathbf{l}\cdot\mathbf{x}_h$, i.e. $\alpha = 0$. We start with no background shear flow considered,

i.e. $\mathbf{b} = 0$. Hence the background linear solution $\overline{\omega}(t)$ is assumed to be zero. The vorticity equation for the plane wave perturbation (31a) takes the form

$$\frac{\partial \omega}{\partial t} + J(\Psi, \omega) + A(t)\mathbf{x} \cdot \nabla \omega + \mathbf{l}^{\perp} \cdot \frac{\partial}{\partial z} \nabla_h^{\perp} \Psi = 0, \qquad (50)$$

where

$$A(t) = \begin{bmatrix} 0 & 0 & 0 \\ 0 & 0 & 0 \\ l_1 & l_2 & 0 \end{bmatrix}. \qquad (51)$$

Then, the vorticity-stream formulation (33a) in the new coordinates ξ become

$$\frac{\partial}{\partial t} \omega(\xi, t) + J(\Psi(\mathbf{x}, t), \omega(\mathbf{x}, t)) + \mathbf{l}^{\perp} \cdot \frac{\partial}{\partial z} \nabla_h^{\perp} \Psi = 0, \qquad (52)$$

with the coordinate transformation in (32) given by

$$\mathbf{X} = e^{\int_0^t A(s)\mathrm{d}s} \xi = \begin{bmatrix} 1 & 0 & 0 \\ 0 & 1 & 0 \\ l_1 t & l_2 t & 1 \end{bmatrix} \xi. \qquad (53)$$

$S(t, \mathbf{k})$ defined in (37) takes the form

$$S(t, \mathbf{k}) = \frac{\mathbf{k_h} \cdot \mathbf{l} - t k_3 \mathbf{l} \cdot \mathbf{l}}{(k_1 - t l_1 k_3)^2 + (k_2 - t l_2 k_3)^2} k_3. \qquad (54)$$

Therefore, the amplitude $\widehat{\omega}_\mathbf{k}(t)$ is computed through the integral of this amplification factor and we then have the following:

PROPOSITION 5   *If the linear vertical velocity is given by $w = \mathbf{l} \cdot \mathbf{x_h}$ and no background shear flow is contained, the exact nonlinear plane wave perturbation solution of the vorticity-stream formulation* (33) *given by*

$$\omega = \widehat{\omega}_\mathbf{k}(t) e^{i\mathbf{k} \cdot \xi} = \widehat{\omega}_\mathbf{k}(t) e^{i(\mathbf{k_h} - k_3 \mathbf{l}t) \cdot \mathbf{x_h} + i k_3 z}, \qquad (55)$$

is unstable and the amplitude demonstrates a "linear" growth for $k_3 \neq 0$

$$\widehat{\omega}_\mathbf{k}(t) = \begin{cases} \widehat{\omega}_\mathbf{k}(0) \sqrt{\dfrac{\mathbf{k_h} \cdot \mathbf{k_h} - 2 k_3 \mathbf{k_h} \cdot \mathbf{l}t + k_3^2 \mathbf{l} \cdot \mathbf{l}t^2}{\mathbf{k_h} \cdot \mathbf{k_h}}} & \text{if } \mathbf{k_h} \neq 0, \\[16pt] \widehat{\omega}_\mathbf{k}(0) t & \text{if } \mathbf{k_h} = 0. \end{cases} \qquad (56)$$

We remind that in this case when $w = \mathbf{l} \cdot \mathbf{x_h}$, the background linear vorticity $\overline{\omega}(t)$ is a constant and assumed to be zero. Hence, the plane wave perturbation (55) is the exact nonlinear solution to the vorticity-stream equation in (20).

We now study the case $b \neq 0$. The vorticity equation (31a) becomes

$$\frac{\partial \omega}{\partial t} + J(\Psi, \omega) + A(t)\mathbf{x} \cdot \nabla \omega + \mathbf{l}^{\perp} \cdot \frac{\partial}{\partial z} \nabla_h^{\perp} \Psi = 0, \qquad (57)$$

with the matrix

$$A(t) = \begin{bmatrix} 0 & -\dfrac{\overline{\omega}(t)}{2} & b_1 \\[2mm] \dfrac{\overline{\omega}(t)}{2} & 0 & b_2 \\[2mm] l_1 & l_2 & 0 \end{bmatrix}. \tag{58}$$

After introducing the characteristic coordinates ξ, (37) and (36) lead to

$$\frac{\mathrm{d}}{\mathrm{d}t}\widehat{\omega}_{\mathbf{k}}(t) = -\frac{\sum_{i,j=1}^{3}\left(l_1\dfrac{\partial\xi_i}{\partial z}\dfrac{\partial\xi_j}{\partial x} + l_2\dfrac{\partial\xi_i}{\partial z}\dfrac{\partial\xi_j}{\partial y}\right)k_i k_j}{\sum_{i,j=1}^{3}\left(\dfrac{\partial\xi_i}{\partial x}\dfrac{\partial\xi_j}{\partial x} + \dfrac{\partial\xi_i}{\partial y}\dfrac{\partial\xi_j}{\partial y}\right)k_i k_j}\widehat{\omega}_{\mathbf{k}}(t), \tag{59}$$

where each derivative term, for example $\partial\xi_i/\partial x$, is an element of the ordered exponential $(\mathrm{e}^{\int_0^t A(s)\mathrm{d}s})^T$. Since no exact solution of (59) can be provided, we integrate it numerically for stability analysis.

Notice that the solution of the ordinary differential equation (ODE) (59) is independent of the magnitude of $\mathbf{k}$. For simplicity, we assume $|\mathbf{k}| = 1$, i.e. $k_1 = \cos\theta_1\cos\theta_2$, $k_2 = \cos\theta_1\sin\theta_2$, and $k_3 = \sin\theta_1$. The following parameters are selected in our numerical simulations: $f = 1$, $\widehat{\omega}_{\mathbf{k}}(0) = 1$. We remind that the Coriolis coefficient f only enters the vorticity-stream formulation (33) for the nonlinear plane wave perturbation implicitly through the background vorticity $\overline{\omega}(t)$. Here since $\alpha = 0$, $\overline{\omega}(t)$ is independent of f, and this is also true for the plane wave perturbation $\widehat{\omega}_{\mathbf{k}}(t)$. The initial background linear vorticity $\bar{\omega}_0$ in (24) is set to zero, as explained at the beginning of this section. Thus, the background linear flow (24) takes the form $\overline{\omega}(t) = (\mathbf{1}^{\perp}\mathbf{b})t$. We consider the following cases.

(a): $\overline{\omega}(t) = 0$, i.e. $\mathbf{l}^{\perp}\cdot\mathbf{b} = 0$.

In this case, we have an explicit form for the ordered exponential

$$\mathrm{e}^{\int_0^t A(s)\mathrm{d}s} = \begin{bmatrix} \dfrac{b_1 l_1 \cosh(\sqrt{D}t) + b_2 l_2}{D} & \dfrac{b_1 l_2 \cosh(\sqrt{D}t) - b_1 l_2}{D} & \dfrac{b_1 \sinh(\sqrt{D}t)}{\sqrt{D}} \\[3mm] \dfrac{b_2 l_1 \cosh(\sqrt{D}t) - b_2 l_1}{D} & \dfrac{b_2 l_2 \cosh(\sqrt{D}t) + b_1 l_1}{D} & \dfrac{b_2 \sinh(\sqrt{D}t)}{\sqrt{D}} \\[3mm] \dfrac{l_1 \sinh(\sqrt{D}t)}{\sqrt{D}} & \dfrac{l_2 \sinh(\sqrt{D}t)}{\sqrt{D}} & \cosh(\sqrt{D}t) \end{bmatrix},$$

where $D = b_1 l_1 + b_2 l_2$. Due to the assumption $\mathbf{l}^{\perp}\cdot\mathbf{b} = 0$, we have $l_1 = D/|\mathbf{b}|\cos\eta$, $l_2 = D/|\mathbf{b}|\sin\eta$, $b_1 = |\mathbf{b}|\cos\eta$, and $b_2 = |\mathbf{b}|\sin\eta$. Here we show numerically that for $D > 0$, growing perturbation occurs, while for $D < 0$, the perturbation is stable for all wave numbers.

First, we consider the case $D > 0$. There are five parameters $D, \eta, |\mathbf{b}|$, and wave numbers θ_1, θ_2. By changing $|\mathbf{b}|$ in a reasonable range, and θ_1, θ_2 from 0 to 2π, we compute the limit of $1/t\log(\widehat{\omega}_{\mathbf{k}}(t))$ as a function of η from 0 to 2π for $D = 1^2, 3^2, 5^2, 7^2$. The results show that the limit is around the level of $\sqrt{D}$; in other words, an unstable perturbation with amplitude $\mathrm{e}^{\sqrt{D}t}$ can be observed. An example for
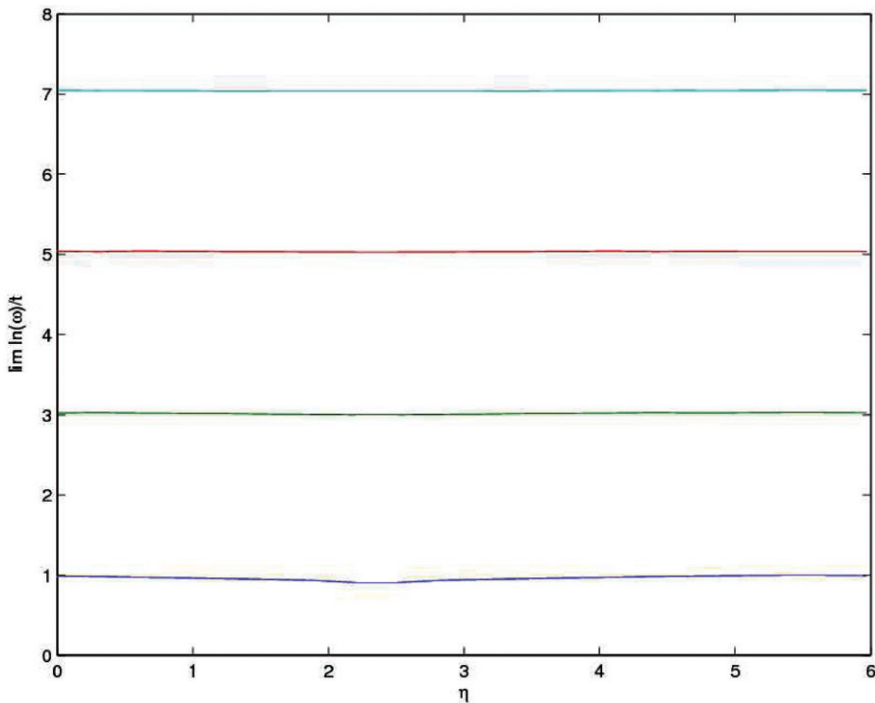
Figure 5. Plot of $\lim_{t\to\infty} 1/t \log(\hat{\omega}_{\mathbf{k}}(t))$, at different D with η changing from 0 to 2π, when $\theta_1 = \pi/8$, $\theta_2 = -\pi/8$, $l_1 = D\cos\eta$, $l_2 = D\sin\eta$, $b_1 = \cos\eta$, $b_2 = \sin\eta$, and $\alpha = 0$.
Notes: From bottom to top: $D = 1, 3^2, 5^2, 7^2$, respectively. Note that the scale is around the level of $\sqrt{D}$.

fixed parameters is presented in figure 5. For a given D, change due to different wave numbers θ_1 and θ_2 is relatively small. Generally, we can observe that the amplitude is of the form $e^{\sqrt{D}t}$. This is reasonable, since in the formula for the transformation matrix $e^{\int_0^t A(s)ds}$ in (60), the elements depend on $\sinh(\sqrt{D}t)$ and $\cosh(\sqrt{D}t)$, which are of the form $e^{\sqrt{D}t}$.

Next we consider the case $D < 0$. Note that $D = 0$ means $\mathbf{l} = 0$ or $\mathbf{b} = 0$, which has already been considered in the first part of this section. By changing $|\mathbf{b}|$ in a reasonable range, and θ_1, θ_2 from 0 to 2π, we compute maximum of the amplitude $\hat{\omega}_{\mathbf{k}}(t)$ for $t \in [0, 100]$ as a function of η from 0 to 2π for $D = -1, -5, -10, -20$. The results show that for all other wave numbers, maximum of $\hat{\omega}_{\mathbf{k}}(t)$ are all relatively small, which seems to be stable. To better understand it, the time history of the amplitude $\hat{\omega}_{\mathbf{k}}(t)$ is presented in figure 6, where a bounded oscillating amplitude is observed.

(b): $\overline{\omega}(t) \neq 0$, i.e. $\mathbf{l}^\perp \cdot \mathbf{b} \neq 0$.

For different sets of fixed $\mathbf{l}$ and $\mathbf{b}$, we compute $\lim_{t\to\infty} 1/t \log(\hat{\omega}_{\mathbf{k}}(t))$ as a function of wave numbers θ_1, θ_2. All results demonstrate an exponential growth. Then for fixed wave numbers θ_1 and θ_2, we compute $\lim_{t\to\infty} 1/t \log(\hat{\omega}_{\mathbf{k}}(t))$, as a function of l_1, l_2, b_1, b_2 in a reasonable range. All of these limits are positive, which imply an exponentially growing amplitude $\hat{\omega}_{\mathbf{k}}(t)$. We then conclude that the plane wave perturbation is unstable with exponential growth in this case.
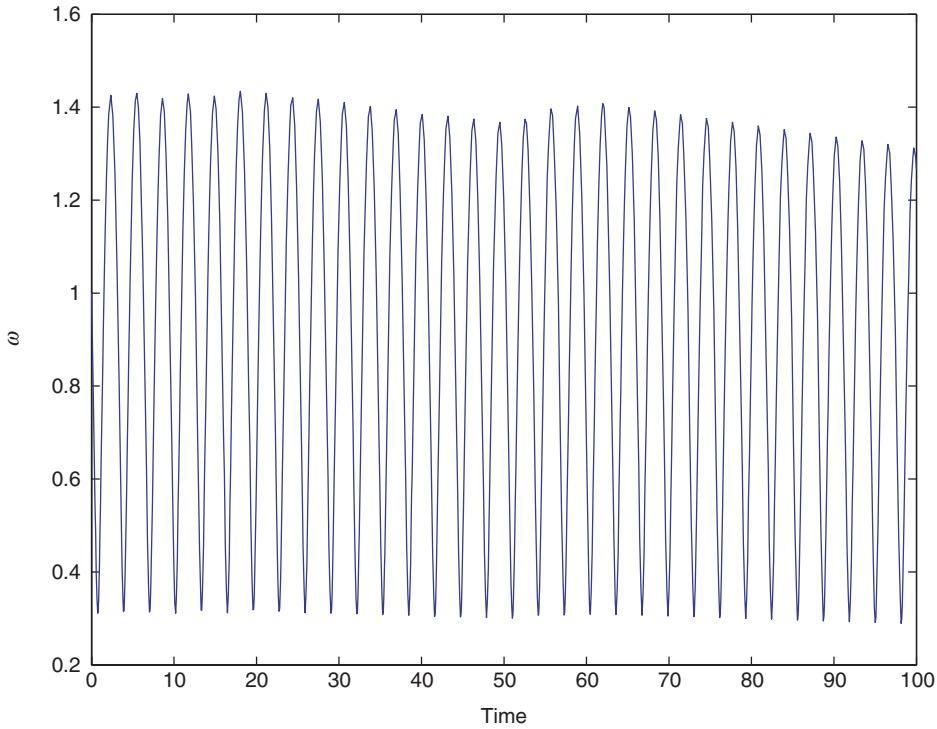
Figure 6. The time history of the amplitude $\hat{\omega}_{\mathbf{k}}(t)$ for $D = -1$, $\eta = 0$, and $|\mathbf{b}| = 1$, when $\alpha = 0$, $\bar{\omega}(t) = 0$, at a fixed wave number $\theta_1 = \pi/4$ and $\theta_2 = 9\pi/10$.

The above numerical study leads to the following:

Summary If the linear heat source is given by $w = \mathbf{l} \cdot \mathbf{x_h}$, numerical tests show that plane wave perturbations always grow exponentially except when $\overline{\omega}(t) = 0$ and $D = \mathbf{l} \cdot \mathbf{b} < 0$.

3.4.5. Case 4: Heat source with both horizontal and vertical dependence and no background shear. We consider the most general linear heat source $w = \mathbf{l} \cdot \mathbf{x_h} + \alpha z$. A simple case when $\mathbf{b} = 0$ is studied in this section. In this case, the vorticity equation for the plane wave perturbation (31a) takes the form

$$\frac{\partial \omega}{\partial t} + J(\Psi, \omega) + A(t)\mathbf{x} \cdot \nabla \omega - \alpha\omega + \mathbf{l}^{\perp} \cdot \frac{\partial}{\partial z} \nabla_h^{\perp} \Psi = 0, \qquad (60)$$

with the matrix

$$A(t) = \begin{bmatrix} -\dfrac{\alpha}{2} & -\dfrac{\overline{\omega}(t)}{2} & 0 \\[2mm] \dfrac{\overline{\omega}(t)}{2} & -\dfrac{\alpha}{2} & 0 \\[2mm] l_1 & l_2 & \alpha \end{bmatrix}. \qquad (61)$$

The coordinate transformation in (32) is given by

$$\mathbf{X} = e^{\int_0^t A(s)ds}\xi = \begin{bmatrix} e^{(\alpha t/2)}\cos(\bar{\theta}(t)) & -e^{(\alpha t/2)}\sin(\bar{\theta}(t)) & \hat{a}_{13}(t) \\ e^{(\alpha t/2)}\sin(\bar{\theta}(t)) & e^{(\alpha t/2)}\cos(\bar{\theta}(t)) & \hat{a}_{23}(t) \\ 0 & 0 & e^{-\alpha t} \end{bmatrix}\xi, \qquad (62)$$

with the coefficients

$$\hat{a}_{13}(t) = \frac{2te^{(\alpha t/2)}\left(e^{-(3\alpha t/2)}(3l_1\alpha t + l_2\bar{\theta}(t)) - \cos(\bar{\theta}(t))(3l_1\alpha t + l_2\bar{\theta}(t)) + \sin(\bar{\theta}(t))(3l_2\alpha t - l_1\bar{\theta}(t))\right)}{9\alpha^2 t^2 + \bar{\theta}^2(t)},$$

$$\hat{a}_{23}(t) = \frac{2te^{(\alpha t/2)}\left(e^{-(3\alpha t/2)}(3l_2\alpha t - l_1\bar{\theta}(t)) + \cos(\bar{\theta}(t))(l_1\bar{\theta}(t) - 3l_2\alpha t) - \sin(\bar{\theta}(t))(3l_1\alpha t + l_2\bar{\theta}(t))\right)}{9\alpha^2 t^2 + \bar{\theta}^2(t)},$$

and

$$\frac{\mathrm{d}}{\mathrm{d}t}\bar{\theta}(t) = \frac{\bar{\omega}(t)}{2}, \quad \bar{\theta}(0) = 0.$$

The vorticity-stream formulation (33a) in the new coordinates ξ becomes

$$\frac{\partial}{\partial t}\omega(\xi, t) + J(\Psi(\mathbf{x}, t), \omega(\mathbf{x}, t)) + \mathbf{l}^\perp \cdot \frac{\partial}{\partial z}\nabla_h^\perp \Psi = 0. \qquad (63)$$

We first discuss the case $\overline{\omega} = 0$, where analytical solution can be obtained. Here $\bar{\theta}(t) = 0$ and the above coefficients reduce to

$$\hat{a}_{13}(t) = \frac{2l_1}{3\alpha}\left(e^{-\alpha t} - e^{-(\alpha t/2)}\right), \quad \hat{a}_{23}(t) = \frac{2l_2}{3\alpha}\left(e^{-\alpha t} - e^{-(\alpha t/2)}\right).$$

$S(t, \mathbf{k})$, defined in (37), takes the form

$$S(t, \mathbf{k}) = \frac{e^{(\alpha/2)t}\mathbf{k_h} \cdot \mathbf{l} + \frac{2k_3}{3\alpha}\left(e^{-\alpha t} - e^{(1/2)\alpha t}\right)\mathbf{l} \cdot \mathbf{l}}{\left(e^{(\alpha/2)t}k_1 + \frac{2l_1}{3\alpha}k_3\left(e^{-\alpha t} - e^{(1/2)\alpha t}\right)\right)^2 + \left(e^{(\alpha/2)t}k_2 + \frac{2l_2}{3\alpha}k_3\left(e^{-\alpha t} - e^{(1/2)\alpha t}\right)\right)^2}$$

$$\times k_3 e^{-\alpha t}. \qquad (64)$$

Plugging this in (36) and integrating, we get

$$\widehat{\omega}_\mathbf{k}(t) = \begin{cases} \widehat{\omega}_\mathbf{k}(0)\sqrt{\dfrac{\left(3\alpha k_1 e^{\alpha t} - 2l_1 k_3\left(e^{\alpha t} - e^{-(1/2)\alpha t}\right)\right)^2 + \left(3\alpha k_2 e^{\alpha t} - 2l_2 k_3\left(e^{\alpha t} - e^{-(1/2)\alpha t}\right)\right)^2}{(3\alpha k_1)^2 + (3\alpha k_2)^2}}, & \text{if } \mathbf{k_h} \neq 0, \\ \widehat{\omega}_\mathbf{k}(0)\left(e^{\alpha t} - e^{-(\alpha/2)t}\right), & \text{if } \mathbf{k_h} = 0. \end{cases}$$

If $\mathbf{k_h} = 0$, instability is observed for both $\alpha > 0$ and $\alpha < 0$. We now discuss the stability for $\mathbf{k_h} \neq 0$ in two different situations.

- $\alpha > 0$ (rising air above, generating a stratiform-type cloud)
  As t approaches infinity, $e^{\alpha t} \to \infty$ and $e^{-\alpha t/2} \to 0$. Hence,

$$\widehat{\omega}_\mathbf{k}(t) \to \widehat{\omega}_\mathbf{k}(0)e^{\alpha t}\sqrt{\frac{(3\alpha k_1 - 2l_1 k_3)^2 + (3\alpha k_2 - 2l_2 k_3)^2}{(3\alpha k_1)^2 + (3\alpha k_2)^2}}. \qquad (65)$$

If $(3\alpha k_1 - 2l_1 k_3)^2 + (3\alpha k_2 - 2l_2 k_3)^2 \neq 0$, $\widehat{\omega}_{\mathbf{k}}(t) \to \infty$, and the perturbation is unstable. If $3\alpha k_1 = 2l_1 k_3$ and $3\alpha k_2 = 2l_2 k_3$, $\widehat{\omega}_{\mathbf{k}}(t) \to \widehat{\omega}_{\mathbf{k}}(0)e^{-\alpha t/2}$, and the perturbation is stable.

- $\alpha < 0$ (descending air above, generating a congestus-type cloud)

  As t approaches ∞, $e^{\alpha t} \to 0$ and $e^{-\alpha t/2} \to \infty$. Hence,

$$\widehat{\omega}_{\mathbf{k}}(t) \to \widehat{\omega}_{\mathbf{k}}(0)e^{-(1/2)\alpha t}\sqrt{\frac{(2l_1 k_3)^2 + (2l_2 k_3)^2}{(3\alpha k_1)^2 + (3\alpha k_2)^2}}. \tag{66}$$

The perturbation is unstable unless $k_3 = 0$ or $\mathbf{l} = 0$. Note that the case $\mathbf{l} = 0$ is already discussed in the previous section, which supports (66).

We have thus shown the following:

PROPOSITION 6 *For a linear heat source $w = \mathbf{l} \cdot \mathbf{x_h} + \alpha z$ with nonzero constants α and $\mathbf{l}$, the plane wave perturbation always grows exponentially except for $\alpha > 0$ along the direction $\mathbf{k} = (2l_1, 2l_2, 3\alpha)$ and for $\alpha < 0$ along the direction $k_3 = 0$, if in the absence of the background linear vorticity $(\overline{\omega}(t) = 0)$ and background shear $(\mathbf{b} = 0)$.*

If $\overline{\omega} \neq 0$, we have the following formula (36) for the amplitude $\widehat{\omega}_{\mathbf{k}}(t)$

$$\frac{\mathrm{d}}{\mathrm{d}t}\widehat{\omega}_{\mathbf{k}}(t) = \alpha\widehat{\omega}_{\mathbf{k}}(t) - \frac{\sum_{i,j=1}^{3}\left(l_1\frac{\partial\xi_i}{\partial z}\frac{\partial\xi_j}{\partial x} + l_2\frac{\partial\xi_i}{\partial z}\frac{\partial\xi_j}{\partial y}\right)k_i k_j}{\sum_{i,j=1}^{3}\left(\frac{\partial\xi_i}{\partial x}\frac{\partial\xi_j}{\partial x} + \frac{\partial\xi_i}{\partial y}\frac{\partial\xi_j}{\partial y}\right)k_i k_j}\widehat{\omega}_{\mathbf{k}}(t)$$

$$= \left(\alpha - \frac{e^{-\alpha t}\sum_{i=1}^{3}\left(l_1\frac{\partial\xi_i}{\partial x} + l_2\frac{\partial\xi_i}{\partial y}\right)k_i k_3}{e^{\alpha t}k_1^2 + e^{\alpha t}k_2^2 + 2\sum_{i=1}^{2}\left(\frac{\partial\xi_i}{\partial x}\hat{a}_{13} + \frac{\partial\xi_i}{\partial y}\hat{a}_{23}\right)k_i k_3 + \left((\hat{a}_{13})^2 + (\hat{a}_{23})^2\right)k_3^2}\right)$$

$$\times \widehat{\omega}_{\mathbf{k}}(t), \tag{67}$$

where each derivative term, for example $\partial\xi_i/\partial x$, is an element of the ordered exponential $(e^{\int_0^t A(s)\mathrm{d}s})^T$. Note that due to the complexity of the ordered exponential $(e^{\int_0^t A(s)\mathrm{d}s})^T$, it is difficult to find the solution of equation (67) explicitly, while we can easily integrate it numerically by an ODE solver.

As before, we assume $k_1 = \cos\theta_1\cos\theta_2$, $k_2 = \cos\theta_1\sin\theta_2$, $k_3 = \sin\theta_1$, and take the parameters $\bar{\omega}_0 = 0$, $f = 1$, $\widehat{\omega}_{\mathbf{k}}(0) = 1$. Two cases are considered.

- $\alpha > 0$ (rising air above, generating a stratiform-type cloud)

  We start by exploring the effect of α. By changing $\mathbf{l} = (l_1, l_2) = L(\cos\eta, \sin\eta)$ in a reasonable range, and θ_2 from 0 to 2π, we compute the limit of $1/t\log(\widehat{\omega}_{\mathbf{k}}(t))$ as a function of θ_1 from 0 to 2π for $\alpha = 1, 2, 3, 4$. The results show that the limit is around the level of α, in other words, an unstable perturbation with amplitude $e^{\alpha t}$ can be observed. An example for fixed parameters is presented in figure 7. For a given α, as L increases, the amplitude increases a little, and the effect of η becomes less important. Changes due to different wave number θ_2 is relatively small. Generally, we can observe that the amplitude is of the form $e^{\alpha t}$.
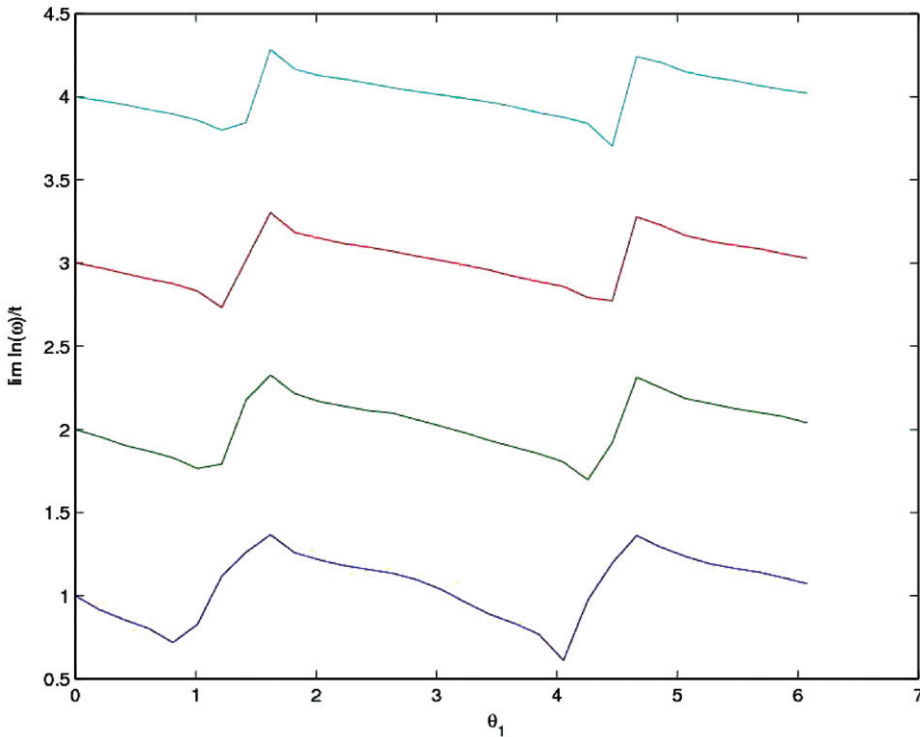
Figure 7. Plot of $\lim_{t \to \infty} 1/t \log(\hat{\omega}_{\mathbf{k}}(t))$ at different α with θ_1 changing from 0 to 2π, when $\theta_2 = \pi/4$, $l_1 = l_2 = 1$, and $\mathbf{b} = 0$.
Notes: From bottom to top: $\alpha = 1, 2, 3, 4$, respectively. Note that the scale is around the level of α.

- $\alpha < 0$ (descending air above, generating a congestus-type cloud)
  As t becomes bigger and bigger, the background vorticity $\bar{\omega}(t) \to -f$, hence, we expect the similar behavior as in the formula (66) for the special case $\bar{\omega} = 0$, i.e. the amplitude is around $e^{-\alpha t/2}$ except at $k_3 = 0$.
  We start by exploring the effect of α. By changing $\mathbf{l} = (l_1, l_2) = L(\cos \eta, \sin \eta)$ in a reasonable range, and θ_2 from 0 to 2π, we compute the limit of $1/t \log(\hat{\omega}_{\mathbf{k}}(t))$ as a function of θ_1 from 0 to 2π for $\alpha = -1, -2, -3, -4$. The results show that an unstable perturbation with amplitude around $e^{-\alpha t/2}$ can be observed for all θ_1 except 0 and π ($k_3 = 0$). For $k_3 = 0$, the amplitude is stable of the form $e^{\alpha t}$. An example for fixed parameters is presented in figure 8. For given α, as L increases, the amplitude increases a little, and the effect of η becomes less important. The change due to a different wave number θ_2 is relatively small. Generally, we can observe that the amplitude is of the form $e^{-\alpha t/2}$ except at $k_3 = 0$ and this confirms our expectation.

3.4.6. Case 5: Heat source with both horizontal and vertical dependence and nonzero background shear.
This is the most general case under the linear vertical velocity assumption. From (33) in full generality, the stability of the perturbation is determined
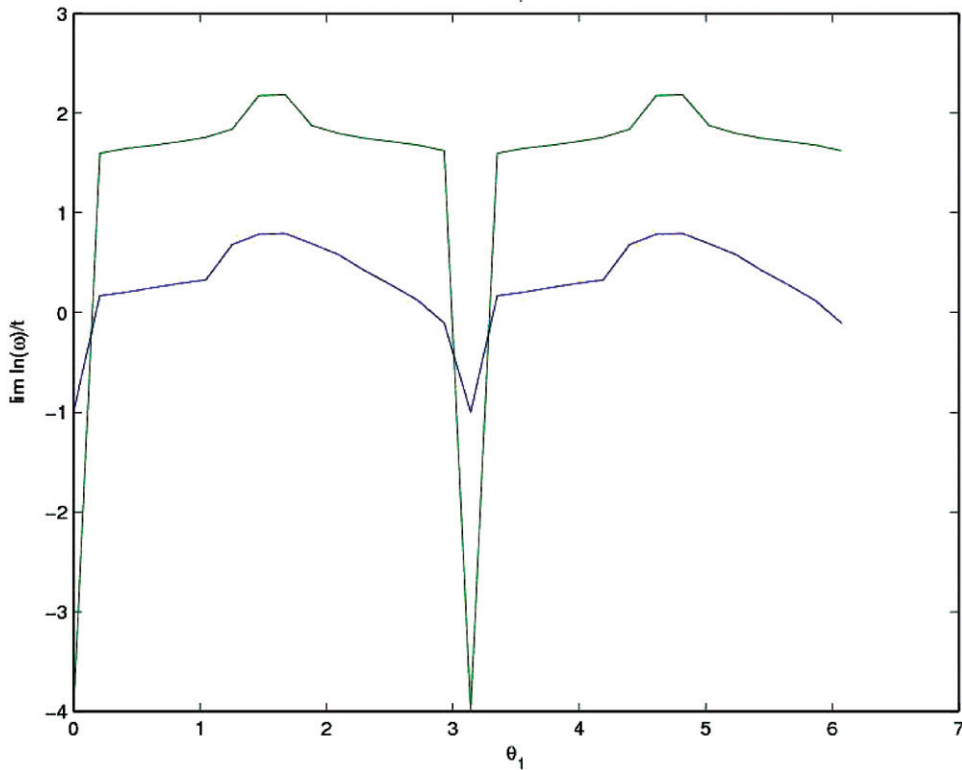
Figure 8. Plot of $\lim_{t \to \infty} 1/t \log(\hat{\omega}_{\mathbf{k}}(t))$ at different α with θ_1 changing from 0 to 2π, when $\theta_2 = \pi/4$, $l_1 = l_2 = 1$, and $\mathbf{b} = 0$.
Notes: From bottom to top: $\alpha = -1$, -4, respectively. Note that the scale is around the level of $-\alpha/2$ except $k_3 = 0$.

by the competition of the stretching term $\alpha\omega$ and the tilting term $\mathbf{l}^{\perp} \cdot \partial/\partial z(\nabla_h^{\perp}\Psi)$, as reflected in (36). These studies are given numerically here.

As earlier, we assume $k_1 = \cos\theta_1\cos\theta_2$, $k_2 = \cos\theta_1\sin\theta_2$, $k_3 = \sin\theta_1$, and take the parameters $\bar{\omega}_0 = 0$, $f = 1$, $\hat{\omega}_{\mathbf{k}}(0) = 1$. Two cases are considered.

- $\alpha > 0$ (rising air above, generating a stratiform-type cloud)

  By changing $\mathbf{l} = (l_1, l_2) = L(\cos\eta_1, \sin\eta_1)$, $\mathbf{b} = (b_1, b_2) = B(\cos\eta_2, \sin\eta_2)$ in a reasonable range, and θ_2 from 0 to 2π, we compute the limit of $1/t\log(\hat{\omega}_{\mathbf{k}}(t))$ as a function of θ_1 from 0 to 2π for $\alpha = 1, 2, 3, 4$. The results show that unstable perturbation with amplitude $e^{\alpha t}$ can be observed. An example for fixed parameters is presented in figure 9. For given α, as L (or B) increases, the amplitude increases a little, and the effect of η_1 (or η_2) becomes less important. The change due to a different wave number θ_2 is relatively small. Generally, we can conclude that the amplitude is of the form $e^{\alpha t}$.

- $\alpha < 0$ (descending air above, generating a congestus-type cloud)

  As we observed in the previous section (case 4), a slight tilting of the heating leads to instability in the absence of shear. Here, we will show that shear may
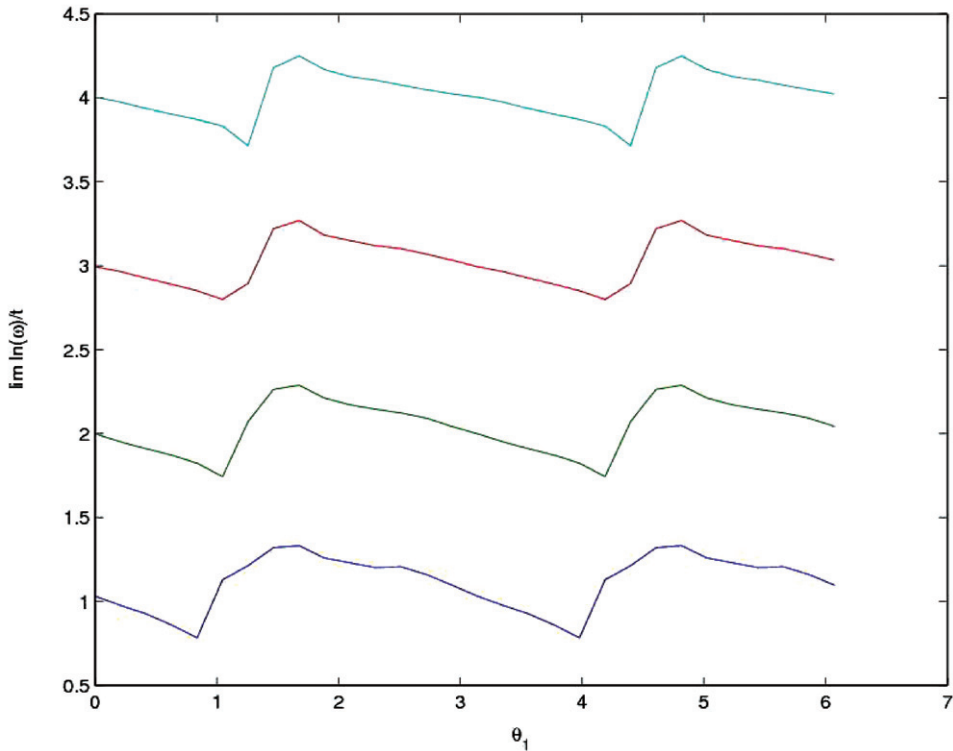
Figure 9.   Plot of $\lim_{t \to \infty} 1/t \log(\hat{\omega}_{\mathbf{k}}(t))$ at different α with θ_1 changing from 0 to 2π, when $\theta_2 = \pi/4$, $\mathbf{l} = (1, 1)$, and $\mathbf{b} = (1, -2)$.
Notes: From bottom to top: $\alpha = 1, 2, 3, 4$, respectively. Note that the scale is around the level of α.

stabilize the flow, and the effect of various parameters on stability will be studied in the following. We remark that based on several numerical experiments, the wave number vector $\mathbf{k}$ does not affect the stability; that is, if the perturbation is stable/unstable for one wave number, it will remain the same for all wave numbers. Hence, all results given below are independent of the wave number.

Figure 10 shows the stable and unstable regions in (b_1, b_2) plane (i.e. based on shear components), where the employed parameters are also given. As it is clearly observed, the plane is divided into two regions by a roughly straight line, hereafter referred to as the regime boundary (RB). The slope of the RB is mainly determined by $\mathbf{l} \cdot \mathbf{b}$ (as will be further confirmed in the following) and as α increases in absolute value [figure 10(b)], the RB shifts to the left with roughly the same slope. Moreover, as α increases in absolute value, the stability region is *increased* in the lower-left region (referred to as A^- where $\mathbf{l} \cdot \mathbf{b}$ is mainly negative), while it is *decreased* in the upper right region (referred to as A^+). Hence, the vertical velocity gradient α has different effects on stability in the two regimes A^+ and A^- identified by the RB. On the other hand, as it is observed in figure 10, the boundaries of the stability regions are mainly straight lines. This means that for fixed $\mathbf{l}$, mainly the *ratio* of b_2/b_1 i.e. direction of shear is
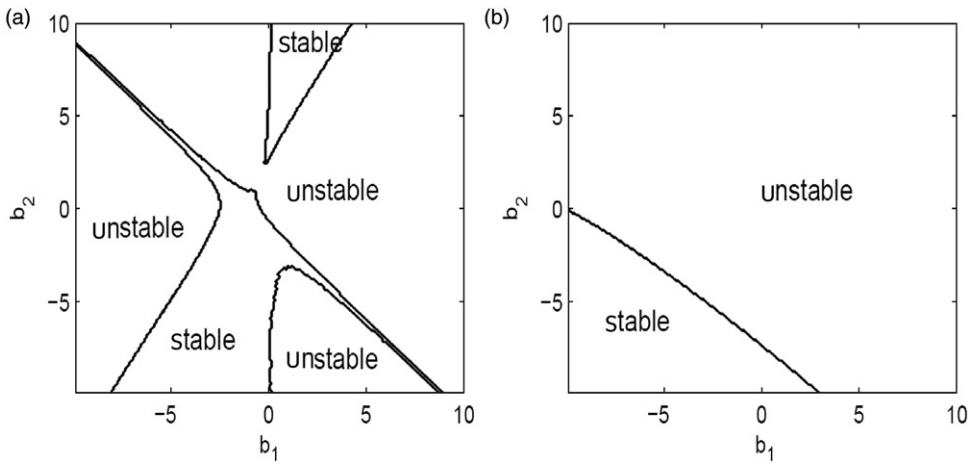
Figure 10. The stability and instability regions in the (b_1, b_2) plane, for $\mathbf{l} = (1, 1)$. (a): $\alpha = -1$; (b): $\alpha = -4$.
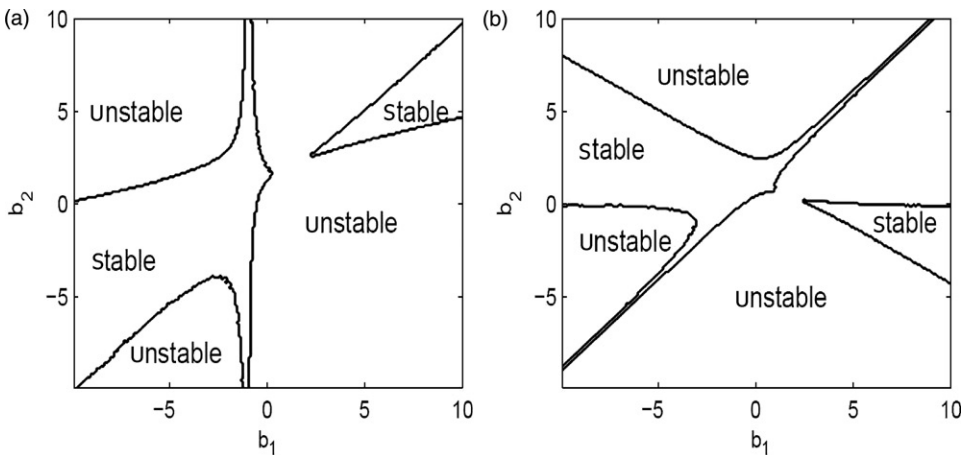

Figure 11. (Same as figure 10) for $\alpha = -1$. (a): $\mathbf{l} = (1, 0)$; (b): $\mathbf{l} = (1, -1)$.

important rather than the individual magnitudes of b_1 and b_2. Finally, note that in figure 10(b), the regions of instability in A^- and stability in A^+ have become smaller and moved to the outside of the shown area due to the effect of α.

In figure 11, we present the regions of stability for fixed α with $\mathbf{l} = (1, 0)$ and $\mathbf{l} = (1, -1)$ where the slope of the RB is roughly 0 and 1, respectively. This strongly confirms that the slope of the RB mainly depends on $\mathbf{l} \cdot \mathbf{b}$. Hence, based on figures 10 and 11, we can conclude that the RB is mainly a straight line identified by $\mathbf{l} \cdot \mathbf{b}$ while α has a shifting effect on the RB. Finally, we examined the effect of the heating tilt $\mathbf{l}$ on the stability region for some fixed $\mathbf{b}$ and variable $\mathbf{l}$. The two regimes A^+ and A^- were again observed, where for fixed $\mathbf{b}$, mainly the ratio of l_2/l_1 i.e. direction of heating tilt was observed to be important, rather than the individual magnitudes of l_1 and l_2 (not shown).
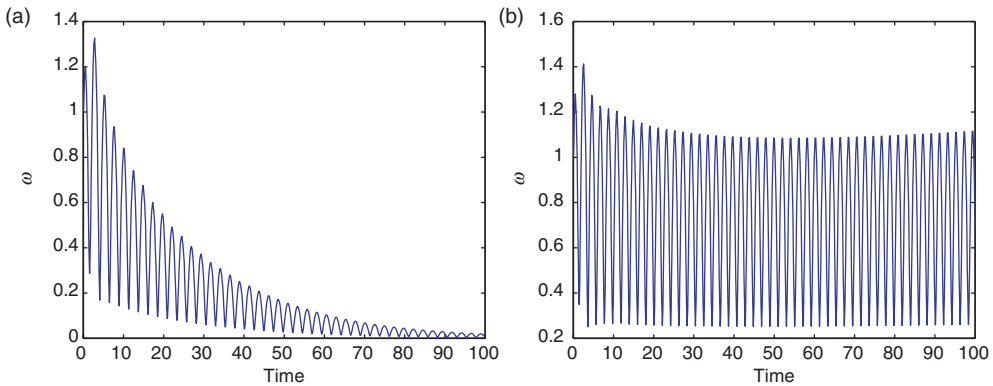
Figure 12.   The time history of the amplitude $\hat{\omega}_{\mathbf{k}}(t)$ at $\theta_1 = \pi/3$, $\theta_2 = \pi/15$ when $\alpha = -1$, $l_2 = 1$, $b_1 = 1$, and $b_2 = 1$; (a): $l_1 = -2.7$; (b): $l_1 = -3.04196$.

Finally, note that in the stable cases, the wave amplitude may decay to zero or stay (oscillating) bounded while in the unstable case, the amplitude may grow linearly or exponentially. The time histories of $\widehat{\omega}_{\mathbf{k}}(t)$ are shown in figure 12, where examples of decaying amplitude (a) and bounded oscillations (b) are presented.

In summary, shear may stabilize the flow and two regimes are identified based on a roughly straight line (called the regime boundary or RB) whose slope is closely related to $\mathbf{l} \cdot \mathbf{b}$, and the vertical velocity gradient α has a stabilizing (destabilizing) effect below (above) RB where $\mathbf{l} \cdot \mathbf{b}$ is mainly negative (positive).

4. Exact radial eddies in a preconditioned background environment

Recent studies (Hendricks *et al.* 2004, Montgomery *et al.* 2006), have revealed the important role of hot towers in cyclogenesis. Montgomery *et al.* (2006) showed how, with the crucial role of vortical hot towers (VHTs), a "midtropospheric cyclonic vortex" may be transformed into a "surface-concentrated (warm core) tropical depression". Hot towers are intense deep convection cores with small horizontal scales (of order 10 km) and short convective lifetimes (of order 1 h) that reach the tropopause via nearly undiluted ascent. They emerge as the preferred coherent structures within the preconditioning mesoscale convective vortex (MCV) embryo (Montgomery *et al.* 2006).

Motivated by the important role of hot towers in the hurricane embryo, it is useful to build elementary models, which exhibit basic characteristics of hot towers to study the evolution of radial eddies (which represent "VHTs") in various radial preconditionings. We will focus on the axisymmetric case, which is a reasonable assumption for hot towers (Montgomery *et al.* 2006). Note that in this section, in general, we are interested in the issue of how heat (mass) sources can generate vortices. We will explore the role of heat sources in cyclogenesis through a reduced form of the asymptotic system (3). Although the terminology of hot towers (cloud scales) is used here, the model that will be presented in this section could be also regarded as an elementary model for larger

(meso) scale systems e.g. mesovortices under synoptic-scale preconditionings. Indeed, as explained in section 2, the canonical equations considered in this article are relevant for both cloud and mesoscales; furthermore also applying uniformly in the equatorial wave guide on somewhat longer timescales (the BMESD model in Majda 2007b).

This section is organized as follows. First, we present the reduced form of the system (3) in the axisymmetric case and split the flow into large-scale mean and small-scale perturbation. We then build some elementary exact large-scale solutions that exhibit some characteristics of various natural situations such as barotropic, deep-convective, and stratiform mean flows. Next, we present an elementary model for hot towers, which represents many characteristics of hot towers such as their general horizontal and vertical features, downdrafts and updrafts, and their life cycles. Using this elementary model, we then study the evolution of hot towers in the absence/presence of various mean flows and briefly discuss the competition of various forcing/preconditioning effects. Note that all numerical studies in this section are in nondimensional units. The dimensionalization for both micro-(cloud) and mesoscales is immediate based on the reference magnitudes given for each scale in section 2.

4.1. *The reduced system in the axisymmetric case*

Here, we present the reduced form of (3) in the axisymmetric case. The flow field is specified by

$$\mathbf{u} = u_r \mathbf{e}_r + u_\theta \mathbf{e}_\theta + w \mathbf{e}_z, \tag{68}$$

where u_r and u_θ are, respectively, radial and tangential velocities, $\mathbf{e}_z$ is the vertical normal vector, and $\mathbf{e}_r$ and $\mathbf{e}_\theta$ are, respectively, the usual radial and tangential normal vectors in cylindrical coordinates where *cyclones in the northern hemisphere* (anti-clockwise eddies) have positive vorticity. For simplicity, we assume $\mathbf{S_u} = 0$, $N^2(z) = 1$ and constant f in (3). Note that axisymmetry is broken in the presence of vertical shear, and hence, no vertical shear is considered here. Under these assumptions, the system (3) is reduced to

$$\frac{\partial u_\theta}{\partial t} + u_r \frac{\partial u_\theta}{\partial r} + u_r \frac{u_\theta}{r} + w \frac{\partial u_\theta}{\partial z} + f u_r = 0, \tag{69a}$$

$$\frac{\partial(r u_r)}{\partial r} + \frac{\partial(r w)}{\partial z} = 0, \tag{69b}$$

$$w = S_\theta. \tag{69c}$$

The first two equations in (69) are the familiar axial momentum and continuity equations in axisymmetric flows, while the last one is the leading-order part of the temperature equation due to a strong heat source, as explained in section 2.

Note that in (69), the vertical velocity $w(r, z, t)$ is determined directly by the given heat source (as before). Further, using (69b), the radial velocity u_r is also directly specified by the heat source

$$u_r = -\frac{1}{r} \int_0^r s \frac{\partial w}{\partial z} \, \mathrm{d}s. \tag{70}$$

That is, when the heat source is strong and axisymmetric, the vertical section of the flow field in (68), i.e. $u_r \mathbf{e}_r + w \mathbf{e}_z$, is totally determined by the heat source. Indeed, we only need to solve a single advection equation with source terms (69a) for u_θ in a given flow field to understand how cyclones/anti-cyclones evolve, and totally specify the flow field (68). This simplicity of the reduced asymptotic model (69) enables us to closely track and understand various effects (production, amplification, dissipation, and advection) and gain some insights into cyclogenesis, which are not so clear and tractable in complex models. In the following, we will show how to reformulate (69) such that the effect of a large-scale preconditioning is also modeled.

4.1.1. The evolution of vertical vorticity. The vertical vorticity ω is related to u_θ through

$$\omega = \frac{1}{r} \frac{\partial (r u_\theta)}{\partial r} = \frac{u_\theta}{r} + \frac{\partial u_\theta}{\partial r}, \tag{71}$$

which is obtained by taking curl (in radial coordinate) of the velocity vector. Hence, (69a) is written equivalently as

$$\frac{\partial u_\theta}{\partial t} + u_r \omega + w \frac{\partial u_\theta}{\partial z} + f u_r = 0. \tag{72}$$

Using (71) and (72), we obtain

$$\frac{\partial \omega}{\partial t} + u_r \frac{\partial \omega}{\partial r} + w \frac{\partial \omega}{\partial z} - \frac{\partial w}{\partial z} (\omega + f) + \frac{\partial w}{\partial r} \frac{\partial u_\theta}{\partial z} = 0. \tag{73}$$

Plugging u_θ and u_r from (71) and (69b) into (73) leads to the following equation for the evolution of vertical vorticity directly in terms of the heat source (w)

$$\frac{\partial \omega}{\partial t} - \left(\frac{1}{r} \int_0^r s \frac{\partial w}{\partial z} \, ds \right) \frac{\partial w}{\partial r} + w \frac{\partial \omega}{\partial z} - \frac{\partial w}{\partial z} (\omega + f) + \frac{\partial w}{\partial r} \frac{\partial}{\partial z} \left(\frac{1}{r} \int_0^r s \omega \, ds \right) = 0. \tag{74}$$

We leave it to the reader to verify that (74) could be also obtained by simplifying the general vorticity equation (16) for the axisymmetric case.

4.1.2. Axisymmetric flow as a superposition of large-scale mean and small-scale perturbation. In this part, our goal is to decompose the axisymmetric flow as a small-scale perturbation added to a large-scale mean flow, which provides a systematic framework to study the evolution of radial eddies generated by (small-scale) hot towers under various (large-scale) preconditionings. We decompose the heat source into a large-scale mean and small-scale perturbation as $S_\theta(t, r, z) = \overline{S}_\theta(t, z) + S'_\theta(t, r, z)$. Hence, the flow quantities are decomposed as

$$w(t, r, z) = \overline{w}(t, z) + w'(t, r, z), \tag{75}$$

$$\omega(t, r, z) = \overline{\omega}(t, z) + \omega'(t, r, z), \tag{76}$$

$$u_\theta(t, r, z) = \overline{u}_\theta(t, r, z) + (u_\theta)'(t, r, z), \tag{77}$$

$$u_r(t, r, z) = \overline{u}_r(t, r, z) + (u_r)'(t, r, z), \tag{78}$$

where $\bar{u}_r$ and $\bar{u}_\theta$ are, respectively, obtained from (70) and (71)

$$\bar{u}_r(t,r,z) = -\frac{1}{2}\frac{\partial \overline{w}(t,z)}{\partial z}r, \tag{79}$$

$$\bar{u}_\theta(t,r,z) = \frac{1}{2}\overline{\omega}(t,z)r. \tag{80}$$

The equation for the evolution of vorticity (73) is simplified for $\overline{\omega}(t,z)$ as

$$\frac{\partial \overline{\omega}(t,z)}{\partial t} + \overline{w}(t,z)\frac{\partial \overline{\omega}(t,z)}{\partial z} = \frac{\partial \overline{w}(t,z)}{\partial z}(\overline{\omega}(t,z) + f). \tag{81}$$

The mean flow satisfies (72) by

$$\frac{\partial \overline{u}_\theta}{\partial t} + \overline{u}_r\overline{\omega} + \overline{w}\frac{\partial \overline{u}_\theta}{\partial z} + f\,\overline{u}_r = 0. \tag{82}$$

Subtracting (82) from (69a), we obtain the following equation for the evolution of small-scale perturbation $(u_\theta)'$ in a large-scale preconditioning (specified by $\overline{w}$, $\overline{u}_r$, and $\overline{\omega}$)

$$\frac{\partial (u_\theta)'}{\partial t} + \left(\overline{u}_r + (u_r)'\right)\left(\frac{\partial (u_\theta)'}{\partial r} + \frac{(u_\theta)'}{r}\right) + (\overline{w} + w')\frac{\partial (u_\theta)'}{\partial z} = -f(u_r)' - (u_r)'\overline{\omega} - w'\frac{\partial \overline{u}_\theta}{\partial z}, \tag{83}$$

where $(u_r)'$ is given by a small-scale heat source using (70). In summary, we have shown the following:

PROPOSITION 7   *For a given heat source* $S_\theta(t,r,z) = \overline{S}_\theta(t,z) + S'_\theta(t,r,z)$, *the system* (69) *has exact solutions of the form* $\mathbf{u} = \bar{\mathbf{u}} + \mathbf{u}'$, *where*

$$\bar{\mathbf{u}} = -\frac{1}{2}\frac{\partial \overline{w}(t,z)}{\partial z}r\mathbf{e}_r + \frac{1}{2}\overline{\omega}(t,z)r\mathbf{e}_\theta + \overline{w}\mathbf{e}_z, \tag{84}$$

$$\mathbf{u}' = -\frac{1}{r}\int_0^r s\frac{\partial w'}{\partial z}\,\mathrm{d}s\mathbf{e}_r + (u_\theta)'\mathbf{e}_\theta + w'\mathbf{e}_z,$$

where $\overline{w} = \overline{S}_\theta$, $w' = S'_\theta$, *and* $\overline{\omega}$ *and* $(u_\theta)'$ *satisfy* (81) *and* (83), *respectively.*

Remark   The term $(\overline{u}_r + (u_r)')\,(u_\theta)'/r$ in (83), is an important term in the evolution of radial eddies. It is an amplification term when $(\overline{u}_r + (u_r)') < 0$, while it is a dissipation term when $(\overline{u}_r + (u_r)') > 0$. This is easily verified by considering the model equation $\partial \varphi / \partial t = \alpha \varphi$ with the solution $\varphi = \varphi_0 \mathrm{e}^{\alpha t}$. This term becomes dominant close to the center-axis where r is very small, and amplifies cyclones and anti-cyclones when the flow direction is toward the center and dissipates them otherwise. For long-time simulations, this term is dominant and overcomes all other source terms.

Note that if the small-scale heat source is removed, the perturbation flow remains stagnant in any vertical section [i.e. $(u_r)' = w' = 0$], and in the absence of mean flow, only a tangential flow remains in the system at a steady state, as explained by (83). Finally, (83) has some properties, which largely reduce the number of cases to be studied. In the absence of the mean flow, and for the initial value $(u_\theta)'_0 = 0$, the dependence of $(u_\theta)'$ on f is linear. Moreover, in the absence of the mean flow, for $f = 0$, the dependence of $(u_\theta)'$ on $(u_\theta)'_0$ is linear. On the other hand, for $f = (u_\theta)'_0 = 0$, the dependence of $(u_\theta)'$ on $\overline{\omega}$ is linear. Further, when $f = 0$, there is a symmetry in the solutions. That is, the results for the case $(u_\theta)'_0 = (\widehat{u}_\theta)'_0$ and $\overline{\omega} = \widehat{\overline{\omega}}$, differ by a (-1) factor from the case $(u_\theta)'_0 = -(\widehat{u}_\theta)'_0$ and $\overline{\omega} = -\widehat{\overline{\omega}}$.

4.1.3. An important special case: steady mean vorticity. In hurricane embryo, the (large-scale) mesovortices provide a vorticity-rich background environment and the life period of hot towers is relatively small compared with the timescales of mesovortices (Montgomery *et al.* 2006), which are called the mean flow here. Therefore, the effect of mesovortices could be realistically modeled by a (quasi) steady mean flow, which corresponds to zero mean vertical velocity (i.e. $\overline{w} = 0$ and hence, $\bar{u}_r = 0$). The mean vorticity equation from (81) in this case is reduced to $\partial\overline{\omega}/\partial t = 0$, or

$$\overline{\omega} = \overline{\omega}_0(z), \tag{85}$$

and because $\overline{w} = \overline{u}_r = 0$, the equation for the perturbation flow (83) is reduced to

$$\frac{\partial(u_\theta)'}{\partial t} + (u_r)'\left(\frac{\partial(u_\theta)'}{\partial r} + \frac{(u_\theta)'}{r}\right) + w'\frac{\partial(u_\theta)'}{\partial z} = -f(u_r)' - (u_r)'\overline{\omega} - w'\frac{\partial\overline{u}_\theta}{\partial z}. \tag{86}$$

Solutions of the reduced system (85) and (86) will be studied in this article for some typical natural situations of specified $\overline{\omega}$. A special case is a *barotropic* steady mean vorticity where $\partial\overline{u}_\theta/\partial z = 0$, and (86) is further simplified to

$$\frac{\partial(u_\theta)'}{\partial t} + (u_r)'\left(\frac{\partial(u_\theta)'}{\partial r} + \frac{(u_\theta)'}{r}\right) + w'\frac{\partial(u_\theta)'}{\partial z} = -f(u_r)' - (u_r)'\overline{\omega}. \tag{87}$$

There is an interesting relation between a barotropic mean vorticity and the Coriolis effect, as explained in the following remark.

Remark The effect of a "barotropic background vorticity" is equivalent to the Coriolis effect. Indeed, the Coriolis parameter could be viewed as a constant barotropic mean vorticity added to a given (not necessarily barotropic) mean vorticity (by replacing $\overline{\omega}$ with $\widetilde{\overline{\omega}} = \overline{\omega} + f$). Although the Coriolis parameter f is not important at the cloud scale, as was mentioned in section 2 and the remark at the beginning of this section, the numerical study presented below equivalently covers the evolution of mesoscale vortices (where f is important). Hence, we prefer to keep the Coriolis parameter f in the discussions below, noting that at the cloud scale, the Coriolis parameter f simply refers to a steady preconditioning barotropic mean vorticity (which may be added to the baroclinic mean vorticity).

We now proceed to the general case $\overline{w} \neq 0$ and obtain the conservation equation of angular momentum for the general case.

4.1.4. The conservation form. Multiplying (69a) by r, and adding a term $u_\theta(\partial(ru_r)/\partial r + \partial(rw)/\partial z)$, which is zero by the continuity equation (69b), we obtain the following conservation equation for the *angular momentum ru_θ*

$$\frac{\partial(ru_\theta)}{\partial t} + \frac{\partial(ru_ru_\theta)}{\partial r} + \frac{\partial(rwu_\theta)}{\partial z} + rfu_r + u_ru_\theta = 0. \tag{88}$$

We now split the angular momentum equation (88) into (large-scale) mean and (small-scale) perturbation. The mean flow satisfies (88) by

$$\frac{\partial(r\overline{u}_\theta)}{\partial t} + \frac{\partial(r\overline{u}_r\overline{u}_\theta)}{\partial r} + \frac{\partial(r\overline{w}\overline{u}_\theta)}{\partial z} + rf\,\overline{u}_r + \overline{u}_r\overline{u}_\theta = 0. \tag{89}$$

Substituting $u_\theta = \overline{u}_\theta + (u_\theta)'$, $w = \overline{w} + w'$, and $u_r = \overline{u}_r + (u_r)'$ in (88) and subtracting (89), we obtain

$$\frac{\partial(r(u_\theta)')}{\partial t} + \frac{\partial(r[\overline{u}_r + (u_r)'](u_\theta)')}{\partial r} + \frac{\partial(r[\overline{w} + w'](u_\theta)')}{\partial z} + rf(u_r)' + [\overline{u}_r + (u_r)'](u_\theta)'$$
$$= -\left[\frac{\partial(r(u_r)'\overline{u}_\theta)}{\partial r} + \frac{\partial(rw'\overline{u}_\theta)}{\partial z} + (u_r)'\overline{u}_\theta\right]. \tag{90}$$

The conservative form (90) will be employed for the numerical studies in this article. Finally, the large-scale mean vorticity (81) could be also written in the conservation form

$$\frac{\partial\overline{\omega}(t,z)}{\partial t} + \frac{\partial[\overline{w}(t,z)\overline{\omega}(t,z)]}{\partial z} = \frac{\partial\overline{w}(t,z)}{\partial z}(2\overline{\omega}(t,z) + f). \tag{91}$$

4.1.5. Numerical scheme and boundary conditions. The large-scale mean flow in the conservation form (91) is solved by a one-dimensional upwind finite volume scheme. A first-order upwind finite volume scheme (in flux form) is then employed to simulate the evolution of perturbation (90) on a staggered grid. A grid of 120×120 computational cells where employed; a uniform vertical spacing is chosen and in the horizontal direction, a variable grid spacing with a very high resolution close to the center is used, which was defined according to $r_j = R(j/N)^4$ where $N = 120$ is the total number of grid points in horizontal direction, r_j is the horizontal coordinate of the jth grid points and $R = 1$ is the radius of the modeled domain. A time step of $\Delta t = 0.01$ was employed. No significant changes were observed with higher temporal or spatial resolutions. Thanks to the flux form of the discretized equations, and noting that the perturbation is compactly supported, the boundary conditions for $r(u_\theta)'$ are easily zero flux at all boundaries.

4.2. *The mean flow*

The case of a steady horizontal mean flow was already studied in section 4.1.3. Here, we present some physical problems of interest for unsteady mean flows (where $\overline{w} \neq 0$), and discuss how various mean (large-scale) heat sources can generate large-scale mean vorticities (radial preconditionings).

Motivated by the most common mean flows in natural events (in particular, the mean flows associated with cyclogenesis), we consider the following cases in this article:

- **Barotropic mean vorticity**
  This case was already discussed in section 4.1.3 and it was shown that the effect of a barotropic mean vorticity is equivalent to the Coriolis effect.
- **Deep convective mean flow**
  In this case, the mean vertical velocity is defined by $\overline{w} = A(t)\sin(\pi z)$, $0 \leq z \leq 1$ and leads to *low-level* cyclone generation, as briefly explained in the following. We remind the reader that, for the mean flow, (81) is reduced to $d\overline{\omega}/dt = (\overline{\omega} + f)\overline{w}_z$ in the characteristic coordinates. This means that the cyclones will spin up if $\overline{w}_z > 0$. In deep convective mean flows,

$\overline{w}_z = \pi A(t)\cos(\pi z)$, which is positive for $z < 1/2$, and negative for $z > 1/2$. This process yields *cyclones in the lower troposphere and anti-cyclones in the upper troposphere*. The vorticity in the steady mean flow that emerges from this process has the form $\overline{\omega}(z) = A\sin(\pi z)$.

- **Stratiform mean flow**
  In this case, the mean vertical velocity is defined by $\overline{w} = -A(t)\sin(2\pi z)$, $0 \le z \le 1$, and *mid-level* cyclone generation is expected; this is because here $\overline{w}_z = -2\pi A(t)\cos(2\pi z)$, which is positive for $1/4 < z < 3/4$ and negative for $z < 1/4$ and $z > 3/4$. This process leads to a *mid-level cyclone and high- and low-level anti-cyclone generation*. The vorticity in the steady mean flow that emerges from such a process has the form $\overline{\omega}(z) = -A\cos(2\pi z)$.

The congestus mean flow has the same $\overline{w}$ as the stratiform case with the opposite sign. Finally, note that another interesting case, is the boundary layer, where $\partial \overline{w}/\partial z > 0$, and yields rising air in mean. This leads to cyclone generation. We do not numerically study this case for the sake of briefness.

4.3. *An elementary model for small-scale hot towers*

In order to study the role of hot towers in the hurricane embryo, we introduce here a perturbation flow with a compact support, which represents basic characteristics of hot towers. The effect of a hot tower is reflected through S'_θ or equivalently through the perturbation vertical velocity w'. Based on the observations (Hendricks *et al.* 2004, Montgomery *et al.* 2006), hot towers exhibit the following basic features: they have a horizontally small-scale *compact support*; their vertical structure resembles *deep convective* rising plumes; they consist of an *intense updraft* in their center and *milder downdrafts* around them, and they exhibit short convective lifetimes including generation, mature, and decaying stages.

Motivated by the above typical features of hot towers, we consider the following profile of vertical velocity as an elementary hot tower model

$$\widehat{w} = \begin{cases} z^4(z-1)^4\left[850r(r-1)^6 + \dfrac{255}{2}(r-1)^6 + 1700r(r-1)^6 \right. \\ \left. \quad + 5100r(r-1)^5 + \dfrac{255}{2r}(r-1)^6 + 765(r-1)^5\right], \qquad 0 \le r, z \le 1, \\ 0 \qquad\qquad\qquad\qquad\qquad\qquad\qquad\qquad\qquad\qquad \text{otherwise.} \end{cases} \tag{92}$$

Using the continuity equation, we obtain

$$\widehat{u_r} = \begin{cases} \left[-4z^3(z-1)^4 - 4z^4(z-1)^3\right]\left(850r^2(r-1)^6 + \dfrac{255}{2}r(r-1)^6\right), & 0 \le r, z \le 1, \\ 0 & \text{otherwise.} \end{cases} \tag{93}$$

The profiles of $\widehat{w}$, $\widehat{u_r}$, and the velocity field in this case are shown in figures 13 and 14, which clearly resemble a deep convective rising plume, with an intense updraft in its center and a mild downdraft around. Note that the above perturbation flow field is compactly supported and satisfies $\widehat{u_r}|_{r=1} = 0$.
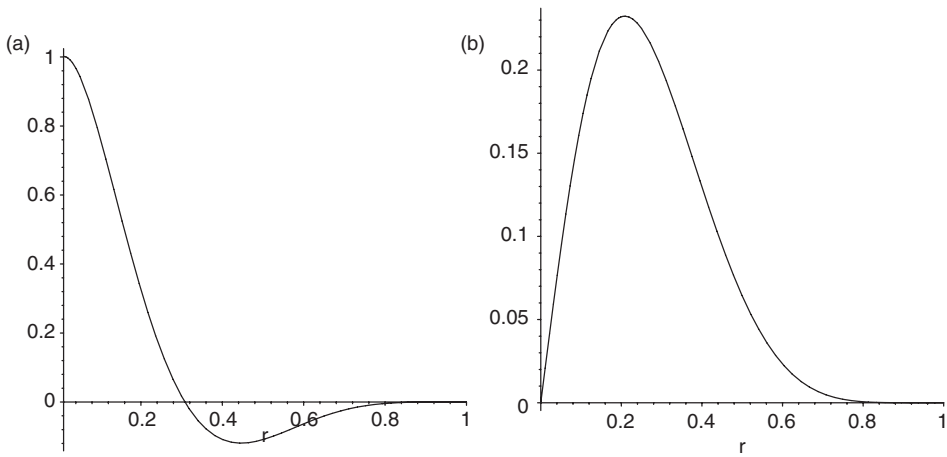
Figure 13.   (a) $\widehat{w}$ at $z = 1/2$ and (b) $\widehat{u}_r$ at $z = 1/2 + \sqrt{7}/14$ where it is maximum, given by (92) and (93).
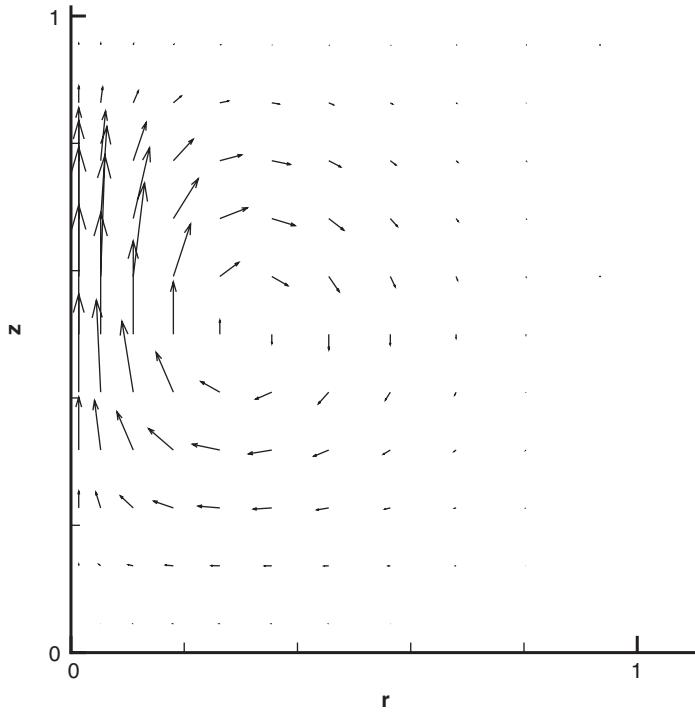

Figure 14.   The perturbation flow field $(\hat{u}_r, \hat{w})$ generated by the hot tower given by (92) and (93).

Finally, the above-mentioned life cycle of a hot tower, may be modeled by the $\sin^+$ function

$$\sin^+(\theta) = \begin{cases} \sin(\theta) & \text{if } \sin(\theta) > 0, \\ 0 & \text{otherwise.} \end{cases} \tag{94}$$

Hence,

$$w' = \widehat{w} \sin^+(\pi t / T_{\max}), \tag{95}$$

$$(u_r)' = \widehat{u_r} \sin^+(\pi t / T_{\max}). \tag{96}$$

In order to study the effect of small-scale preconditioning, in some cases below we will consider the natural choice of a small-scale barotropic vortex as initial condition

$$(u_\theta)'(t = 0, r, z) = \begin{cases} (u_\theta)'_0, & 0 \le r, z \le 1, \\ 0 & \text{otherwise}, \end{cases} \tag{97}$$

where value of $(u_\theta)'_0$ is variable in the numerical experiment (the case $(u_\theta)'_0 = 0$ corresponds to no initial perturbation). Note that positive $(u_\theta)'_0$ corresponds to cyclonic initial small-scale vorticity. To give insight about various possible cases, numerical studies are performed here for short ($T_{\max} = 1$) and long ($T_{\max} = 10$) events. In the following, we study the evolution of radial eddies in various radial preconditionings. We begin with the evolution of hot towers under no mean flow, and then the effect of a steady mean flow on hot towers is studied.

4.4. *Evolution of hot towers in the absence of mean flows*

Here, we assume no background rotation ($\overline{\varpi} = 0$ and $\overline{w} = 0$). This gives an insight into how initial conditions and the Coriolis parameter can affect the evolution of a hot tower in the absence of mean flow. The equation (83) for the evolution of $(u_\theta)'$ in this case is reduced to

$$\frac{\partial (u_\theta)'}{\partial t} + (u_r)' \left(\frac{\partial (u_\theta)'}{\partial r} + \frac{(u_\theta)'}{r} \right) + w' \frac{\partial (u_\theta)'}{\partial z} = -f(u_r)'. \tag{98}$$

Note that the effects of the terms $-f(u_r)'$ and $(u_r)'(u_\theta)'/r$ depend on the sign of $(u_r)'$. Due to the special form of the perturbation flow field (92) and (93), $(u_r)' < 0$ for $z < 1/2$, and $(u_r)' > 0$ for $z > 1/2$, which leads to the following effects:

- The source term $-f(u_r)'$ generates cyclones i.e. positive tangent velocity $(u_\theta)'$ in the lower troposphere ($z < 1/2$) and anti-cyclones i.e. negative $(u_\theta)'$ in the upper troposphere. In the following, the effect of this term will be referred to as the "Coriolis effect".
- The term $(u_r)'(u_\theta)'/r$ is an amplification term when $z < 1/2$ and a dissipation term when $z > 1/2$ (see the remark in section 4.1.2). The effect of this term will be referred to as "amplification effect" or "dissipation effect". In the regions close to center, where r is very small, this term is dominant.

4.4.1. Evolution of hot towers with no small-scale initial vorticity. This case is called case A1: In this case, the system is linear in terms of the Coriolis parameter f, and hence, we only consider $f = 1$. Because no initial $(u_\theta)'$ is assumed, at the beginning only the "Coriolis effect" is active and generates cyclones and anti-cyclones in the lower and upper troposphere, respectively. The generated cyclones and anti-cyclones are then advected by the perturbation flow, which lead to positive tangent velocity
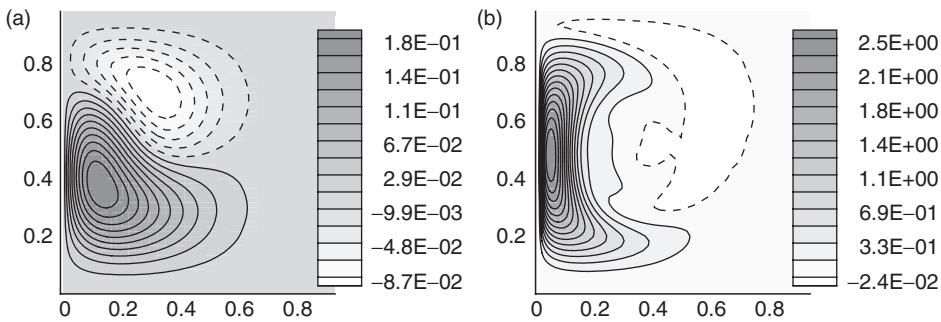
Figure 15. Case A1, contour plots of $(u_\theta)'$ for $(u_\theta)'_0 = 0$, $f = 1$, results at $t = T_{max}$ for $T_{max} = 1$ (a) and $T_{max} = 10$ (b).
Notes: Dashed lines show negative values (anti-cyclonic flow). Horizontal axis is r and vertical axis is z.

$(u_\theta)'$ i.e. cyclonic flow close to the center and negative $(u_\theta)'$ i.e. anti-cyclonic flow far from the center. Then, the ''amplification effect'' leads to a huge increase of $(u_\theta)'$ in the inner core. This effect becomes more and more dominant as time increases and $(u_\theta)'$ is increased extremely rapidly in the internal core around mid-levels. The huge $(u_\theta)'$ generated at the inner core, is advected to the higher levels and is dissipated there. Note that if the simulation time is considered long enough, then the amplification and advection effects overcome the dissipation effect and a cyclonic flow is generated in a main part of the inner core. However, $(u_\theta)'$ at the high levels remains negative for a long time because the advection effect is small at that part and it takes a long time for advection and amplification effects to overcome the Coriolis effect in that region. The upper anti-cyclone is advected far from the center and it becomes weaker. This does not violate the conservation of angular momentum because the conserved quantity in (88) is actually $r(u_\theta)'$ and hence, $(u_\theta)'$ becomes small as r is increased. We call this regime "the Coriolis-dominated regime". contour plots of the tangent velocity $(u_\theta)'$ at $t = T_{max}$ for $T_{max} = 1$ and 10, are shown in figure 15. The negative $(u_\theta)'$ (e.g. anti-cyclonic vortex) is very small in absolute value. Note that in figure 15, the cyclonic tangent velocity generated by an order 1 Coriolis effect, is of order 0.1 for $T_{max} = 1$ and of order 1 for $T_{max} = 10$. Hence, by increasing the simulation time by one order of magnitude, the dominant generated vortices (here, cyclones) are roughly amplified by one order. This feature is roughly observed in most other experiments presented below.

We now briefly discuss the evolution of vertical vorticity. The initial vorticity is produced in the domain according to the term $\partial w'/\partial z f$ in the vorticity equation (73). As the time increases, a huge vorticity is produced close to the center. This is because the vorticity is given by $\partial(u_\theta)'/\partial r + (u_\theta)'/r$; in the regions close to the center, the term $(u_\theta)'/r$ is dominant (because r is very small) and this leads to a huge vorticity in the inner core.

4.4.2. The effect of a nonzero small-scale initial vorticity when $f = 0$. This case is called case A2: In this case, the system is linear in terms of $(u_\theta)'_0$, and thus, we only consider $(u_\theta)'_0 = 1$. That is, initially we have a cyclonic perturbation here. The amplification, dissipation, and advection effects are active, since the beginning of simulation
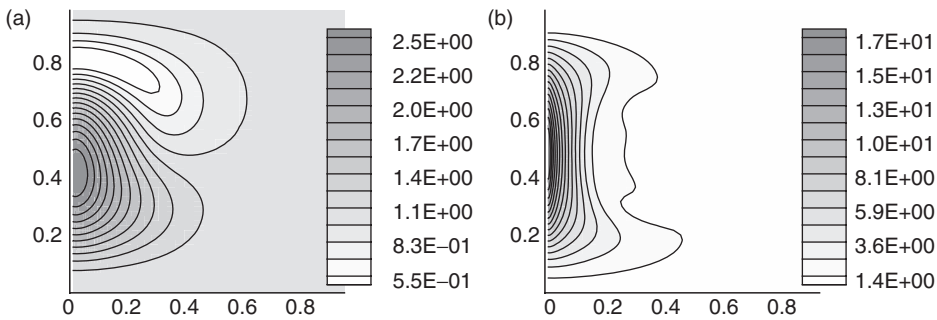
Figure 16.   Case A2, contour plots of $(\mu_\theta)'$ for $(u_\theta)'_0 = 1$, $f = 0$, results at $t = T_{\max}$ for $T_{\max} = 1$ (a) and $T_{\max} = 10$ (b).
Note: Horizontal axis is r, and vertical axis is z.

(because $(u_\theta)'_0 \neq 0$), and as before a strong cyclonic flow in the inner core at mid-levels is generated. However, due to the absence of the Coriolis effect here, no anti-cyclonic flow is generated and the whole flow swirls cyclonicly. We call this regime "the initial vorticity-dominated regime". Typical contour plots of $(u_\theta)'$ for this case are given in figure 16. We remind the reader that since the system is linear in terms of $(u_\theta)'_0$, if the initial $(u_\theta)'_0$ is negative, then anti-cyclones are amplified and the whole flow swirls as anti-cyclone. Note that in the previous case (the Coriolis-dominated regime), both cyclonic and anti-cyclonic flows were generated, but in the present regime, depending on the initial condition, only cyclonic or anti-cyclonic flow is generated. Finally, in figure 16, the cyclonic tangent velocity generated by an order 1 initial tangent velocity, is of order 1 for $T_{\max} = 1$ and of order 10 for $T_{\max} = 10$. Hence, compared to the previous case, we conclude that the effect of an initial tangent velocity of order 1, is roughly one order of magnitude stronger than the effect of an order 1 Coriolis forcing. Further, comparing the two cases $T_{\max} = 1$ and $T_{\max} = 10$, for the cases A1 and A2, we observe that the flow generated in case A1 grows more rapidly in time compared with case A2. This is because the Coriolis effect is a source term and it is active during the simulation.

4.4.3. The competition of Coriolis and initial small-scale vorticity.   In order to see how the initial small-scale cyclones/anti-cyclones and the Coriolis parameter f compete, here we select a small initial perturbation $(u_\theta)'_0 = \pm 0.05$ and change f in the range $0 \leq f \leq 1$. The reason for selecting small $(u_\theta)'_0$ is that, as explained earlier, the effect of $(u_\theta)'_0$ is of one order of magnitude stronger than the effect of Coriolis. For larger $(u_\theta)'_0$, the Coriolis effect cannot compete and the flow field is dominated by the initial small-scale vorticity. Here, for small values of f, e.g. $f = 0.1$ *the initial condition is dominant* and the results are qualitatively similar to those of the case A2, while for large values of f, e.g. $f = 1$, *the Coriolis effect is dominant* and the results are close to those of the case without initial condition (case A1). We now discuss the two cases of cyclonic and anti-cyclonic initial small-scale flows separately.

- **Cyclonic initial small-scale vorticity**
  This case is called case A3. Typical contour plots of $(u_\theta)'$ for $(u_\theta)'_0 = 0.05$ when $f = 0.5$ are given in figure 17. Note that, here Coriolis and initial small-scale
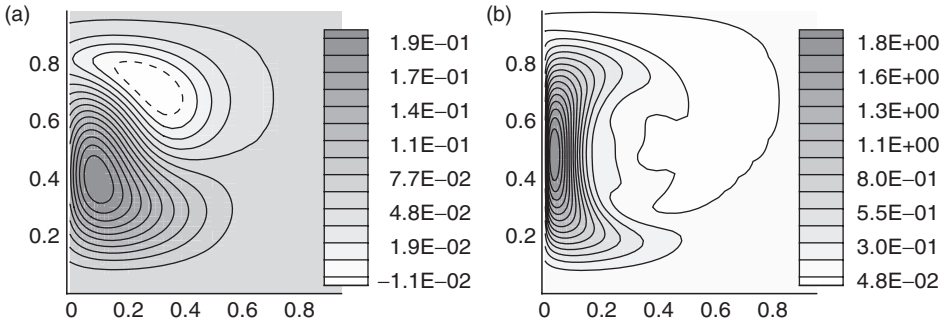
Figure 17.   Case A3, contour plots of $(\mu_\theta)'$ for $(u_\theta)'_0 = 0.05$, $f = 0.5$, results at $t = T_{max}$ for $T_{max} = 1$ (a) and $T_{max} = 10$ (b).
Note: Horizontal axis is r, and vertical axis is z.

vorticity collaborate in the lower levels, but they have opposite effects in higher levels. Comparing figure 17(b) with figure 16(b), we observe that the high-level anti-cyclone is largely weakened in figure 17, due to the opposite effect at high levels. Moreover, although the Coriolis is reduced in figure 17, the low-level cyclone is of almost at the same strength due to the collaboration at low levels.

- **Anti-cyclonic initial small-scale vorticity**
  This case is called case A4. Typical contour plots of $(u_\theta)'$ for $(u_\theta)'_0 = -0.05$ when $f = 0.5$ are given in figure 18. Note that for $f = 0.5$, although for short timescales the small-scale initial vorticity is dominant and generates an anti-cyclonic flow, for longer timescales the Coriolis effect wins, and starts to generate a cyclone as time increases. This is because, as explained earlier, cyclones/anti-cyclones generated in case A1 (due to Coriolis) grow more rapidly in time compared with case A2. In figure 18, an anti-cyclone is observed in the center due to initial condition, then followed by a cyclone due to Coriolis effect, then followed by an anti-cyclone due to Coriolis (compare with figure 15).

4.5. *The effect of steady mean flows on hot towers*

In this part, we study the evolution of hot towers in presence of a steady mean flow, which was introduced in section 4.1.3. For simplicity, we assume zero initial small-scale vorticity e.g. $(u_\theta)'_0 = 0$. We remind that the equation (83) in this case ($\overline{w} = \overline{u}_r = 0$) is reduced to (86), which we repeat here

$$\frac{\partial (u_\theta)'}{\partial t} + (u_r)'\left(\frac{\partial (u_\theta)'}{\partial r} + \frac{(u_\theta)'}{r}\right) + w'\frac{\partial (u_\theta)'}{\partial z} = -f(u_r)' - (u_r)'\overline{\omega} - w'\frac{\partial \overline{u}_\theta}{\partial z}.$$

Note that for $f = 0$, and in the absence of initial small-scale vorticity, the solution is linear in $\overline{\omega}$. Due to the presence of the terms $-f(u_r)' - (u_r)'\overline{\omega} - w'\partial \overline{u}_\theta/\partial z$, the tangential velocity $(u_\theta)'$ will be generated in the system, even with a zero initial condition. As mentioned in a remark in section 4.1.3, the natural choice of a barotropic background vorticity returns to the previous case (case A; no background rotation).
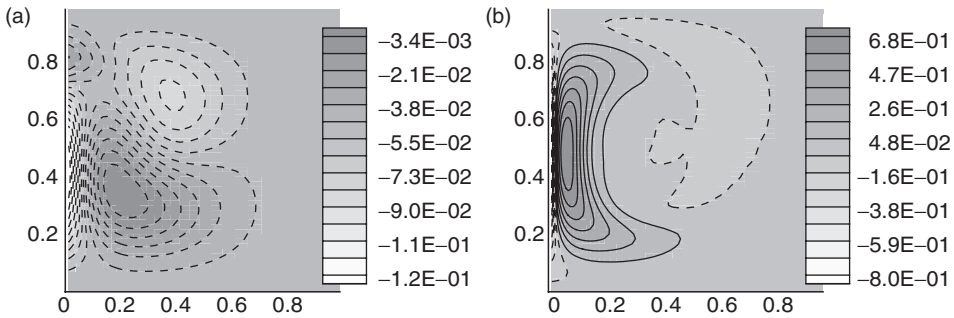
Figure 18. Case A4, contour plots of $(\mu_\theta)'$ for $(u_\theta)'_0 = 0.05$, $f = 0.5$, results at $t = T_{max}$ for $T_{max} = 1$ (a) and $T_{max} = 10$ (b).

Note: Horizontal axis is r, and vertical axis is z.

Hence, motivated by the mean vorticity generated only due to the deep convective and stratiform mean flows in section 4.2, we will consider here four cases of mean vorticity as large-scale preconditioning. Experiments in this section are grouped as case B.

4.5.1. Low-level cyclonic and high-level anti-cyclonic mean flow. This case is called case B1. The mean vorticity here corresponds to the build up from a transient large-scale deep convective flow (section 4.2) and it is defined by $\overline{\omega} = \sin(2\pi z)$.

- When $f = 0$, at the beginning, both terms $-(u_r)'\overline{\omega}$ and $-w'\partial\overline{u}_\theta/\partial z$ are active. Note that the term $\partial\overline{u}_\theta/\partial z$ linearly increases with r, and w' is large at mid-levels. Hence, the term $-w'\partial\overline{u}_\theta/\partial z$ is dominant in the mid-levels at outer region (far from center) and leads to anti-cyclonic flow. Another component of the mean flow effect, i.e. $-(u_r)'\overline{\omega}$, is dominant close to the center (in the outer region it is small compared with $-w'\partial\overline{u}_\theta/\partial z$ because $\partial\overline{u}_\theta/\partial z$ increases with r). Due to the special form of the perturbation flow, $-(u_r)'\overline{\omega}$ is always positive here and tends to generate cyclonic flow. This, along with the amplification effect, leads to cyclone in the inner core for $T_{max} = 1$. The cyclone in the internal part is much stronger than the anti-cyclone in the external part due to the amplification effect. We call this case the "deep convective mean flow-dominated regime". For the case $T_{max} = 10$, the term $(u_r)'(u_\theta)'/r$ becomes dominant again as in the previous cases and forces the flow to swirl mainly as a *cyclone* at mid-levels with a small anti-cyclonic flow far from the center at low- to mid-levels.
- As f is increased, the inner cyclone is amplified as explained in the following. We remind the reader that the Coriolis term could be included in the mean vorticity through a change of variable $\widetilde{\omega} = \overline{\omega} + f$, and hence they collaborate when have the same sign. Here the Coriolis effect and the background mean vorticity have similar effects at low levels. Thus, stronger cyclones (compared to the case $f = 0$) are generated there and then transported to the inner core. Hence, the inner cyclone is amplified by increasing f. In short times, i.e. $T_{max} = 1$, the anti-cyclone becomes weaker as f is increased, because Coriolis effect and the background mean vorticity do not act exactly at same regions. For $T_{max} = 10$, the Coriolis effect and the background mean vorticity totally collaborate, and
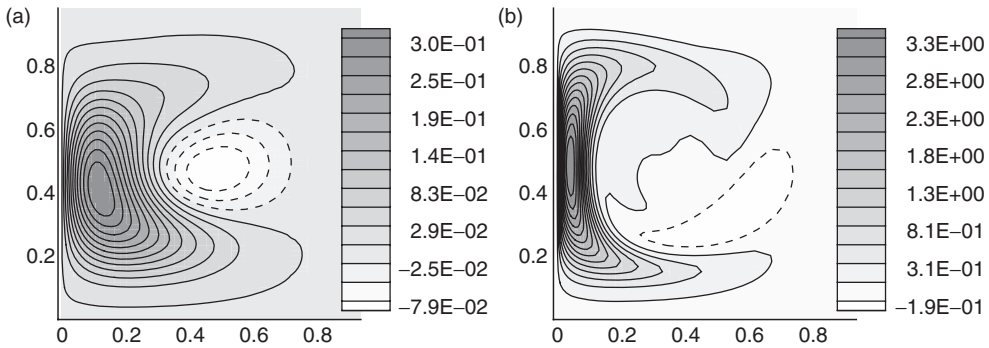
Figure 19. Case B1, contour plots of $(\mu_\theta)'$ for $(u_\theta)'_0 = 0$, $f = 0.5$, results at $t = T_{\max}$ for $T_{\max} = 1$ (a) and $T_{\max} = 10$ (b).
Notes: Dashed lines show negative values (anti-cyclonic flow). Horizontal axis is r and vertical axis is z.

by increasing f, the final inner cyclone is almost linearly amplified. As expected, when f is increased, the results become more and more similar to the case $\overline{\omega} = 0$, which was already identified as Coriolis-dominated regime.

Typical contour plots of $(u_\theta)'$ for this case when $f = 0.5$ are given in figure 19. The strength of cyclones are comparable to case A1 by a 1.5 factor, which is expectable due to the relation between f and a barotropic vorticity and noting that $\overline{\omega} + f$ is of order 1.5 here. The anti-cyclonic tangent velocity is roughly two order weaker as expected due to the discussion above.

4.5.2. Low-level anti-cyclonic and high-level cyclonic mean flow. This case is called case B2. Here, the mean vorticity generated by a transient large-scale downward flow (section 4.2) is considered, which is defined by $\overline{\omega} = -\sin(2\pi z)$.

- When $f = 0$, the results are linear in terms of $\overline{\omega}$, and differ from the last case by a (-1) factor.
- As f is increased, the Coriolis effect and the background mean vorticity act oppositely and the inner anti-cyclone eventually becomes a cyclone as in the Coriolis-dominated regime. An interesting case is $f = 0.5$, where the two effects (mean vorticity and Coriolis) are close and this lead to an anti-cyclone in the inner core, followed by a cyclone, while low- and high-level flows are still cyclonic for $T_{\max} = 10$. Typical contour plots of $(u_\theta)'$ for this case when $f = 0.5$ are given in figure 20. For $T_{\max} = 1$, the strength of anti-cyclones are comparable by a -0.8 factor to the strength of cyclones in case A1, which is again reasonable. For $T_{\max} = 10$, both cyclones and anti-cyclones are amplified by a factor 5 and they are propagated in the domain due to advection.

4.5.3. Mid-level cyclone and low- and high-level anti-cyclone. This case is called case B3. Motivated by the mean vorticity generated by transient effects from a large-scale stratiform flow (section 4.2), here we choose $\overline{\omega} = -\cos(2\pi z)$.
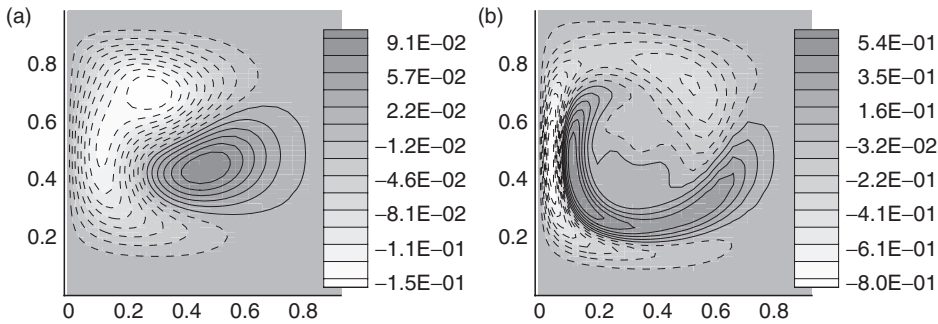
Figure 20. Case B2, contour plots of $(\mu_\theta)'$ for $(u_\theta)'_0 = 0$, $f = 0.5$, results at $t = T_{\max}$ for $T_{\max} = 1$ (a) and $T_{\max} = 10$ (b).
Notes: Dashed lines show negative values (anti-cyclonic flow). Horizontal axis is r and vertical axis is z.

- When $f = 0$, in the case $T_{\max} = 1$, low-level anti-cyclones and high-level cyclones are generated in the inner core due to the term $-(u_r)'\overline{\omega}$, followed by low-level cyclones and high-level anti-cyclones in the outer region (far from center) due to the term $-w'\partial \overline{u}_\theta / \partial z$ (not shown). When $T_{\max} = 10$, an internal anti-cyclone is generated (around the center) while a cyclone is generated in the external region (when $f = 0$). We call this case the "stratiform mean flow-dominated regime".

- As f is increased, the flow evolves as following. For the case $T_{\max} = 1$, the cyclones and anti-cyclones in the *internal* region become much weaker (because they do not collaborate with the Coriolis-dominated regime) and the external ones move toward the center. For the case $T_{\max} = 10$, by increasing the Coriolis parameter, the internal anti-cyclone becomes much weaker and the external cyclone becomes stronger, and the flow field becomes closer to the Coriolis-dominated regime, as expected. Typical contour plots of $(u_\theta)'$ for this case when $f = 0.5$ are given in figure 21. Note that a small spot of weak low-level anti-cyclonic flow (close to center) at $T_{\max} = 1$, becomes much amplified and generates an anti-cyclonic inner core. This is a general important feature due to the amplification effect. Indeed, in the long run, the flow direction (cyclonic/ anti-cyclonic) in the inner core is only dictated by the flow direction at the lowest level. Finally, comparing figure 21 with figure 19, we observe that the cyclones generated by a deep convective mean flow (case B1), are two times stronger than those generated by stratiform mean flow (case B3). Hence, *deep convective preconditionings should have a higher potential for initiation of hurricanes*. Anti-cyclones are stronger here compared with case B1. Moreover, the strength of cyclones and anti-cyclones are closer to each other in this case compared to deep convective mean flows (case B1).

4.5.4. Mid-level anti-cyclone and low- and high-level cyclone. This case is called case B4. The mean vorticity generated by a transient large-scale congestus flow is considered here, which differs by a (-1) factor from the stratiform flow in section 4.2), and defined by $\overline{\omega} = \cos(2\pi z)$.

- When $f = 0$, the results differ from the last case by a (-1) factor, due to linearity in $\overline{\omega}$.

Figure 21. Case B3, contour plots of $(\mu_\theta)'$ for $(u_\theta)'_0 = 0$, $f = 0.5$, results at $t = T_{max}$ for $T_{max} = 1$ (a) and $T_{max} = 10$ (b).

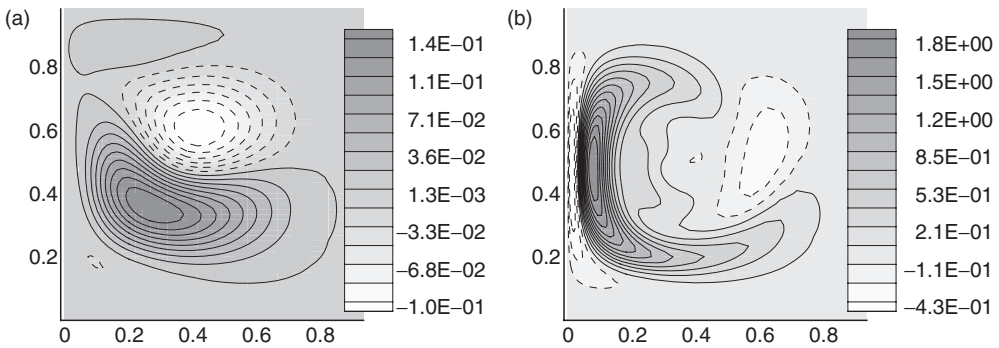Notes: Dashed lines show negative values (anti-cyclonic flow). Horizontal axis is r and vertical axis is z.

Figure 22. Case B4, contour plots of $(\mu_\theta)'$ for $(u_\theta)'_0 = 0$, $f = 0.5$, results at $t = T_{max}$ for $T_{max} = 1$ (a) and $T_{max} = 10$ (b).

Notes: Dashed lines show negative values (anti-cyclonic flow). Horizontal axis is r and vertical axis is z.
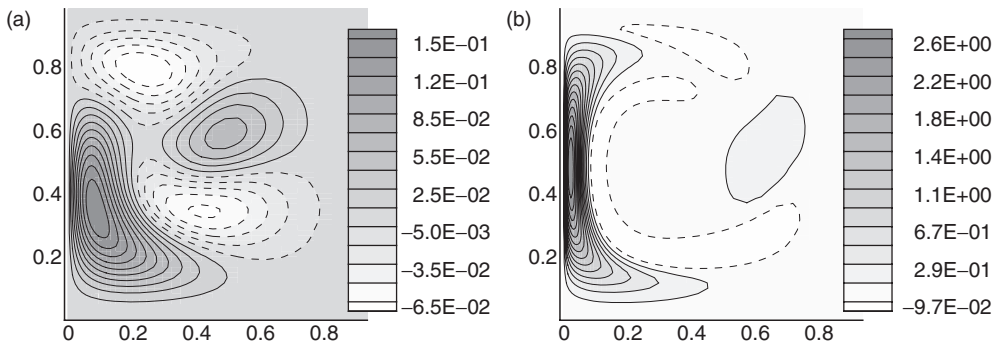
- As f is increased, the flow evolves as following. In the case $T_{max} = 1$, the cyclones and anti-cyclones in the *external* region become much weaker (due to the Coriolis effect). When $T_{max} = 10$, by increasing the Coriolis parameter, the internal cyclone becomes much stronger and the external anti-cyclone becomes weaker. Typical contour plots of $(u_\theta)'$ for this case for $f = 0.5$ are given in figure 22. Compared with the last case, B3, although the flow features are different, the strength of cyclones are still comparable, but anti-cyclones are much weaker here. For the long time $T_{max} = 10$, the cyclonic/anti-cyclonic regions are exchanged, as expected. Hence, congestus preconditionings also have less potential for initiation of hurricanes, compared with deep convective preconditionings.

Remark In the presence of a nonzero initial small-scale vorticity, the competition of the Coriolis effect, initial small-scale vorticity, and various large-scale steady mean flows governs the evolutions of radial eddies. The flow field in this case evolves based on the combination of various regimes identified above, which is beyond the scope of this article.

4.6. *The effect of an unsteady mean flow on hot towers*

Here, we briefly explain the effect of an unsteady mean flow ($\overline{w} \neq 0$). The mean flow in most natural cases evolves much slower than the perturbation. Hence, the quasi-steady state assumption for the mean vorticity made above is still reasonable. However, the advection, amplification, and dissipation effects are based on the total velocities $\overline{u}_r + (u_r)'$ and $\overline{w} + w'$. Further, the small-scale radial eddies $(u_\theta)'$ generated due to hot towers do not remain in the system at a steady state after the end of the perturbation heating. This is because the terms involving mean radial and vertical velocities $\overline{u}_r$ and $\overline{w}$ in (83) are still active and hence, the evolution of $(u_\theta)'$ continues even after the decay of the hot tower ($w' = (u_r)' = 0$). The mean flow in this case advects $(u_\theta)'$ in the system and also amplifies (dissipates) it when the flow direction is toward (outward) the center, through the term $\overline{u}_r(u_\theta)'/r$ in (83). Hence, the radial eddies generated by the hot towers may be even further amplified by the mean flow.

4.7. *Large-scale linear flows with sheared sertical structure*

There is a direct link between the large-scale linear flows from proposition 1 in section 3 and the large-scale vertical flows in proposition 7 of this section. Both can be generalized for nonlinear, nonaxisymmetric mean flows as following:

PROPOSITION 8   *For a large-scale heat source $S_\theta = \overline{S}_\theta(t,z)$, the system (3) has exact solutions of the form*

$$\overline{w}(t,z) = \overline{S}_\theta(t,z),$$
$$\overline{\mathbf{u}}_h(z,t) = \frac{1}{2}\overline{\omega}\mathbf{x}_h^{\perp} + \frac{1}{2}\mathcal{D}_h\mathbf{x}_h - \frac{1}{2}\overline{w}_z\mathbf{x}_h + \overline{\mathbf{b}}(z,t), \tag{99}$$

where $\mathcal{D}_h$ is an arbitrary 2×2 symmetric matrix with zero trace;

$$\mathcal{D}_h = \begin{pmatrix} \gamma_1(t,z) & \gamma_2(t,z) \\ \gamma_2(t,z) & -\gamma_1(t,z) \end{pmatrix},$$

$\overline{\mathbf{b}}(z,t)$ is an arbitrary background shear flow and $\overline{\omega}$ satisfies

$$\frac{\partial\overline{\omega}(t,z)}{\partial t} + \overline{w}(t,z)\frac{\partial\overline{\omega}(t,z)}{\partial z} = \frac{\partial\overline{w}(t,z)}{\partial z}(\overline{\omega}(t,z) + f). \tag{100}$$

Proof   Noting that

$$\nabla_h \times \left(\frac{1}{2}\overline{\omega}\mathbf{x}_h^{\perp}\right) = \overline{\omega}, \quad \nabla_h \cdot \left(-\frac{1}{2}\overline{w}_z\mathbf{x}_h\right) = -\overline{w}_z, \tag{101}$$

and the term $1/2\mathcal{D}\mathbf{x_h} + \mathbf{b}(z,t)$ is horizontally curl and divergence free, for a given $\overline{\omega}$ and $\overline{w}(t,z)$, it is straightforward to check that the velocity field given by (99) satisfies the continuity equation in (3), and moreover, $\nabla_h \times \overline{\mathbf{u}}_h = \overline{\omega}$. Finally, (100) guarantees that the momentum equation in (3) is also satisfied.

4.8. *Summary*

The evolution of the perturbation flow $(u_\theta)'$ for the case of a steady-mean vorticity is governed by (86) through the terms $(u_r)'(u_\theta)'/r$, $w'\partial(u_\theta)'/\partial z$, $f(u_r)'$, $(u_r)'\overline{\omega}$, $w'\partial\overline{u}_\theta/\partial z$, and

the advection effects. For small time ($T_{max} = 1$), the competition of the initial condition, Coriolis, and the mean vorticity determines the flow regime (based on the above terms), and may lead to several cyclones and anti-cyclones. For long time ($T_{max} = 10$), the dominant term is $(u_r)'(u_\theta)'/r$. It always amplifies the cyclones and anti-cyclones when the flow direction is toward the center, and dissipates them when the flow direction is outward. Hence, in the hot tower perturbation flow considered here, this term acts as an amplification term in the bottom, and as a dissipation term in the top. Therefore, for long-time simulations ($T_{max} \gg 1$), the final cyclonic/anti-cyclonic situation depends on flow conditions in the lowest level; if the lowest level swirls cyclonicly, then in the whole domain, a mainly cyclonic flow is generated, and vice versa. That is, if the competition of various effects in short times lead to a cyclonic flow at the lower level, independent of the flow structure at higher levels, eventually a cyclonic flow is developed in the system and vice versa.

In the case of an unsteady mean flow, the radial eddies are also advected by the mean flow. Moreover the amplification/dissipation term becomes $(\bar{u}_r + (u_r)')(u_\theta)'/r$ and the amplification/dissipation effect is now determined by the direction of the total radial velocity $\bar{u}_r + (u_r)'$.

In summary, in presence of initial small-scale vorticity, Coriolis, or mean vorticity, hot towers (heat sources) can generate very large vorticities in their core through the term $(\bar{u}_r + (u_r)')(u_\theta)'/r$, and the role of a barotropic mean vorticity is equivalent to the Coriolis effect. Finally, hot towers appear to generate stronger cyclonic flows with the deep convective preconditioning compared with stratiform/congestus preconditionings.

5. Concluding remarks

In this article, we presented a comprehensive study of a canonical balanced model, which involves vertically sheared horizontal flows with mass sources arising in several multi-scale models for the tropics. In section 2, we developed two new examples of physical regimes for the balanced models, which are useful for the hurricane embryo; a comprehensive multi-scale model for this process is developed elsewhere (Majda *et al.* 2008).

First, when the heat source is specified as a linear function, general linear flow solutions are introduced as background large-scale preconditioning fields. Nonlinear plane wave perturbations for vertical vorticity in such a preconditioned environment are studied through a combination of exact solutions and elementary numerics. The stability analysis reveals how these vorticity perturbations grow due to the effects of a linear heat source and background shear flow. An interesting result comes from the case when $\alpha < 0$ (the linear heat source is given by $w = \alpha z + \mathbf{l} \cdot \mathbf{x_h}$). If the heating is independent of horizontal coordinates (i.e. $\mathbf{l} = 0$), the perturbation is stable everywhere, as it is well known. However, if the heating starts to depend on horizontal coordinates, the flow field becomes unstable in most cases.

Next, by constructing an elementary axisymmetric model of hot towers (which represents their basic characteristics), it was shown how a heat/mass source can generate large vorticity in a suitable preconditioning. Useful elementary insight into the

role of hot towers in cyclogenesis has been obtained through combination of exact solutions and simple numerics. The simplicity of the reduced models enabled us to carefully study and understand the role of various effects in generation, amplification, and dissipation of vorticity in hot towers. Various cases were studied, which showed how several regimes of cyclonic/anti-cyclonic flow could happen due to the effect of various natural background large-scale preconditioning, the Coriolis forcing, and initial small-scale cyclonic/anti-cyclonic vorticity. Section 4.7 provides a summary.

Although the terminology of hot towers and cloud scales are used here, the canonical model studied in this article, is also relevant for larger scales, and the elementary model study also gives insight into how mesovortices may be generated due to the heat sources by mesoscale convective systems under various synoptic-scale preconditionings.

The insights obtained in this study, are useful as elementary structures in multi-scale models for the hurricane embryo (Majda *et al.* 2007), where hot towers play a substantial role (Hendricks *et al.* 2004, Montgomery *et al.* 2006). These will be developed elsewhere in a subsequent study.

References

Ackerman, S.A. and Knox, J.A., *Meteorology: Understanding the Atmosphere*, 2003 (Brooks Cole: Stamford, CT).
Bayly, B.J., Holm, D.D. and Lifschitz, A., Three-dimensional stability of elliptical vortex columns in external strain flows. *Phil. Trans. R. Soc. Lond. A*, 1996, **354**, 895–926.
Biello, J.A. and Majda, A.J., A new multiscale model for the Madden-Julian oscillation. *J. Atmos Sci.*, 2005, **62**, 1694–1721.
Biello, J.A. and Majda, A.J., Modulating synoptic scale convective activity and boundary layer dissipation in the IPESD models of the Madden-Julian oscillation. *Dyn. Atmos. Oceans*, 2006, **42**, 152–215.
Biello, J.A., Majda, A.J. and Moncreiff, M., Meridional momentum flux and super rotation in the multi-scale IPESD MJO model. *J. Atmos. Sci.*, 2007, **64**, 1636–1651.
Craik, A.D.D., The stability of unbounded two- and three-dimensional flows subject to body forces: some exact solutions. *J. Fluid Mech.*, 1989, **198**, 275–292.
Craik, A.D.D. and Allen, H.R., The stability of three-dimensional time-periodic flows with spatially uniform strain rates. *J. Fluid Mech.*, 1992, **234**, 613–628.
Craik, A.D.D. and Criminale, W.O., Evolution of wavelike disturbances in shear flows: a class of exact solutions of the Navier-Stokes equations. *Proc. R. Soc. Lond. A*, 1986, **406**, 13–26.
Embid, P.F. and Majda, A.J., Low Froude number limiting dynamics for stably stratified flow with small or fixed Rossby Number. *Geophys. Astrophys. Fluid Dyn.*, 1998, **87**, 1–50.
Fincham, A.M., Maxworthy, T. and Spedding, G.R., The horizontal and vertical structure of the vorticity field in freely-decaying, stratified grid. *Dyn. Atmos. Oceans*, 1996, **23**, 153–169.
Julien, K., Knobloch, E., Milliff, R. and Werne, J., Generalized quasi-geostrophy for spatially anisotropic rotationally constrained flows. *J. Fluid Mech.*, 2006, **555**, 233–274.
Hendricks, E.A., Montgomery, M.T. and Davis, C.A., The role of ''vortical'' hot towers in the formation of tropical cyclone diana. *J. Atmos. Sci.*, 2004, **61**, 1209–1232.

Klein, R., Asymptotic analyses for atmospheric flows and the construction of asymptotically adaptive numerical methods. *Z. Angew. Math. Mech.*, 2000, **80**, 765–777.

Klein, R. and Majda, A.J., Systematic multiscale models for deep convection on mesoscales. *Theo. Comp. Fluid Dyn.*, 2006, **20**, 525–551.

Lifschitz, A. and Hameiri, E., Local stability conditions in fluid dynamics. *Phys. Fluids A*, 1991, **3**, 2644–2651.

Majda, A., *Introduction to PDEs and Waves for the Atmosphere and Ocean,* Volume 9 of Courant Lecture Notes in Mathematics, 2003 (New York: AMS/CIMS).

Majda, A., Multiscale models with moisture and systematic strategies for super parameterization. *J. Atmos. Sci.*, 2007a, **64**, 2726–2734.

Majda, A., New multiscale models and self-similarity in tropical convection. *J. Atmos. Sci.*, 2007b, **64**, 1393–1404.

Majda, A. and Grote, M., Model dynamics and vertical collapse in decaying strongly stratified flows. *Phys. Fluids*, 1997, **9**, 2932–2940.

Majda, A. and Klein, R., Systematic multiscale models for the tropics. *J. Atmos. Sci.*, 2003, **60**, 393–408.

Majda, A., Mohammadian, M. and Xing, Y., *Multiscale equations for the hurricane embryo in a WTG environment*, 2008, in preparation.

Majda, A. and Shefter, M.G., The instability of stratified flows at large Richardson numbers. *Proc. Natl. Acad. Sci. USA*, 1998, **95**, 7850–7853.

Mapes, B.E., Tulich, S., Lin, J.-L. and Zuidema, P., The mesoscale convection life cycle: building block or prototype for large-scale tropical waves?. *Dyn. Atmos. Oceans*, 2006, **42**, 3–29.

Montgomery, M.T., Nicholls, M.E., Cram, T.A. and Saunders, A.B., A vortical hot tower route to tropical cyclogenesis. *J. Atmos. Sci.*, 2006, **63**, 355–386.

Pedlosky, J., *Geophysical Fluid Dynamics*, 1979 (New York: Springer).

Riley, J.J. and Lelong, M.-P., Fluid motions in the presence of strong stable stratification. *Annu. Rev. Fluid Mech.*, 2000, **32**, 613–657.

Smith, L.M., Numerical study of two-dimensional stratified turbulence. In *Advances in Wave Interaction and Turbulence,* Contemp. Math. 283, edited by P.A. Milewski, L.M. Smith, F. Wale and E.G. Tabak, pp. 91–106, 2001 (Providence, RI: Amer. Math. Soc.).

Smith, L.M. and Waleffe, F., Generation of slow large-scales inforced rotating stratified turbulence. *J. Fluid Mech.*, 2002, **451**, 145–168.

Smith, R.K. (editor), *The Physics and Parametrization of Moist atmospheric Convection*, Volume 505 of NATO Advanced Study Institute Series C. Mathematical and Physical Sciences, 1997 (Norwell, MA: Kluwer).

Sobel, A.H., Nilsson, J. and Polvani, L.M., The weak temperature gradient approximation and balanced tropical moisture waves. *J. Atmos. Sci.*, 2001, **58**, 3650–3665.

Waite, M.L. and Bartello, P., Stratified turbulence dominated by vortical motion. *J. Fluid Mech.*, 2004, **517**, 281–308.

Appendix A

We now present the details for deriving the linear exact solutions for vertically sheared horizontal flow with heat source. Let us assume that the Coriolis parameter f is constant and source terms S_θ is linear. $\mathbf{S_u}$ is ignored.

A.1 *Vorticity solution*

We assume that

$$w = S_\theta = \alpha(t)z + \mathbf{l}(t) \cdot \mathbf{x}_h, \tag{A.1}$$

for an arbitrary $\mathbf{l}$ and α as functions of t only, which implies

$$\triangle_h \Phi = -\alpha, \quad \nabla_h^\perp w = \mathbf{l}^\perp. \tag{A.2}$$

Since our purpose is to find the linear solution of the system, velocity u_h are linear functions in space, which means that vorticity ω only depends on t. Hence,

$$\triangle_h \Psi = \omega(t). \tag{A.3}$$

Then, based on relations A.2 and A.3, it is natural to assume that Ψ and Φ are both independent of z.

Starting from equation (16), inserting the Helmholtz decomposition and using the linear formula of w (A.1), we have the new equation for vorticity

$$\frac{\partial \omega}{\partial t} - \alpha \omega + \mathbf{l}^{\perp} \cdot \frac{\partial \mathbf{b}(z, t)}{\partial z} - \alpha f = 0. \tag{A.4}$$

A.2 *Symmetric and antisymmetric analysis*

We first introduce the notation

$$V_1 = \begin{pmatrix} \dfrac{\partial u}{\partial x} & \dfrac{\partial u}{\partial y} \\ \dfrac{\partial v}{\partial x} & \dfrac{\partial v}{\partial y} \end{pmatrix}, \quad V_1^{\perp} = \begin{pmatrix} -\dfrac{\partial v}{\partial x} & -\dfrac{\partial v}{\partial y} \\ \dfrac{\partial u}{\partial x} & \dfrac{\partial u}{\partial y} \end{pmatrix}, \quad P_1 = \begin{pmatrix} p_{xx} & p_{xy} \\ p_{xy} & p_{yy} \end{pmatrix}.$$

Since we only consider the linear solution, V_1 defined above is only a function of time t. Further, we can decompose $\mathbf{u}$ as

$$\mathbf{u}_h = V_1(t)\mathbf{x}_h + \mathbf{b}z,$$

where $\mathbf{b} = \mathbf{b}(t)$ refers to the shear flow $(\partial u/\partial z \quad \partial v/\partial z)^T$.

Compute the derivative w.r.t. x, y of the momentum equation and have

$$\frac{\mathrm{d}}{\mathrm{d}t} V_1 + V_1^2 + \begin{pmatrix} \dfrac{\partial u}{\partial z} \\ \dfrac{\partial v}{\partial z} \end{pmatrix} \begin{pmatrix} \dfrac{\partial w}{\partial x} & \dfrac{\partial w}{\partial y} \end{pmatrix} + fV_1^{\perp} = -P_1. \tag{A.5}$$

Using the fact that $\partial V_1/\partial t = \mathrm{d}V_1/\mathrm{d}t$ (coming from the linearity of $\mathbf{u_h}$), the above equation can be simplified as

$$\frac{\partial}{\partial t} V_1 + V_1^2 + \mathbf{b}\mathbf{l}^T + fV_1^{\perp} = -P_1. \tag{A.6}$$

We then decompose V_1 into its symmetric part $\mathcal{D}_1$ and antisymmetric part Ω_1, where $\Omega_1 = 1/2 \begin{pmatrix} 0 & -\omega \\ \omega & 0 \end{pmatrix}$. Using the fact that $V_1^2 = \mathcal{D}_1^2 + \Omega_1^2 + \Omega_1\mathcal{D}_1 + \mathcal{D}_1\Omega_1$ where the first two terms are symmetric and the latter two are antisymmetric, we can break up the velocity gradient equation (A.6) to the symmetric part

$$\frac{\partial}{\partial t}\mathcal{D}_1 + \mathcal{D}_1^2 + \Omega_1^2 + \frac{1}{2}(\mathbf{l}\mathbf{b}^T + \mathbf{b}\mathbf{l}^T) + \frac{f}{2}(V_1^{\perp} + (V_1^{\perp})^T) = -P_1, \tag{A.7}$$

and the antisymmetric part

$$\frac{\partial}{\partial t}\Omega_1 + \mathcal{D}_1\Omega_1 + \Omega_1\mathcal{D}_1 + \frac{1}{2}(\mathbf{b}\mathbf{l}^T - \mathbf{l}\mathbf{b}^T) + \frac{f}{2}(V_1^{\perp} - (V_1^{\perp})^T) = 0, \tag{A.8}$$

which can be further simplified to be the vorticity equation (A.4).

At the end, we take the derivative w.r.t. the z direction of the momentum equation

$$\frac{\partial}{\partial t}\frac{\partial u}{\partial z} + u\frac{\partial}{\partial x}\frac{\partial u}{\partial z} + v\frac{\partial}{\partial y}\frac{\partial u}{\partial z} + w\frac{\partial}{\partial z}\frac{\partial u}{\partial z} + \frac{\partial u}{\partial x}\frac{\partial u}{\partial z} + \frac{\partial u}{\partial y}\frac{\partial v}{\partial z} + \frac{\partial u}{\partial z}\frac{\partial w}{\partial z} - f\frac{\partial v}{\partial z} = -p_{xz}, \tag{A.9}$$

$$\frac{\partial}{\partial t}\frac{\partial v}{\partial z} + u\frac{\partial}{\partial x}\frac{\partial v}{\partial z} + v\frac{\partial}{\partial y}\frac{\partial v}{\partial z} + w\frac{\partial}{\partial z}\frac{\partial v}{\partial z} + \frac{\partial v}{\partial x}\frac{\partial u}{\partial z} + \frac{\partial v}{\partial y}\frac{\partial v}{\partial z} + \frac{\partial v}{\partial z}\frac{\partial w}{\partial z} + f\frac{\partial u}{\partial z} = -p_{yz}. \tag{A.10}$$

These can be simplified into the form

$$\mathbf{b}_t + (V_1 + \alpha I)\mathbf{b} + f\mathbf{b}^\perp = -(p_{xz} \quad p_{yz})^T. \tag{A.11}$$

A.3 *Proposition*

Here, we present a full version of the proposition with the pressure term included.

PROPOSITION 9 *For the vertically sheared horizontal flow with heat source*

$$\frac{\mathrm{d}}{\mathrm{d}t}\mathbf{u_h} + f\mathbf{u_h}^\perp = -\nabla_h p,$$
$$\nabla_h \cdot \mathbf{u_h} + w_z = 0,$$
$$w = S_\theta,$$

with f a fixed constant representing the Coriolis effect and S_θ a linear function of $\mathbf{x}$, z, *there are exact linear solutions of the form*

$$w = S_\theta = \mathbf{l} \cdot \mathbf{x}_h + \alpha z, \ \ with \ \mathbf{l} = (l_1(t), l_2(t))^T, \ \alpha = \alpha(t), \tag{A.12a}$$

$$\bar{\mathbf{u}}_h = -\frac{\alpha}{2}\mathbf{x}_h + \frac{1}{2}\bar\omega(t)\mathbf{x}_h^\perp + \mathcal{D}_h(t)\mathbf{x}_h + \mathbf{b}z, \ \ with \ \mathbf{b} = (b_1(t), b_2(t))^T, \tag{A.12b}$$

$$p = \frac{1}{2}P(t)\mathbf{x} \cdot \mathbf{x}. \tag{A.12c}$$

where $\mathcal{D}_h$ is an arbitrary 2×2, traceless, symmetric matrix, $\mathbf{b} = (b_1(t), b_2(t))^T$ is a vector describing the background shear and $\bar\omega(t) = \nabla_h \times \bar{\mathbf{u}}_h$ satisfies

$$\frac{\partial\overline\omega}{\partial t} = \alpha(\overline\omega + f) - \mathbf{l}^\perp \cdot \mathbf{b}, \quad \overline\omega(0) = \overline\omega_0. \tag{A.13}$$

Matrix $P(t)$ is given by

$$\begin{pmatrix} P_1(t)_{2\times 2} & P_2(t) \\ P_2(t)_{1\times 2}^T & p_{22}(t) \end{pmatrix},$$

with $p_{22}(t)$ as an arbitrary function of t and

$$\begin{aligned} -P_1 &= \frac{\mathrm{d}\mathcal{D}}{\mathrm{d}t} + \mathcal{D}_1^2 + \Omega_1^2 + \frac{1}{2}(\mathbf{l}\mathbf{b}^T + \mathbf{b}\mathbf{l}^T) + \frac{f}{2}\left(V_1^\perp + (V_1^\perp)^T\right), \\ -P_2 &= \mathbf{b}_t + (V_1 + \alpha I)\mathbf{b} + f\mathbf{b}^\perp, \end{aligned} \tag{A.14}$$

where $V_1 = \mathcal{D}_1 + \Omega_1$, $\Omega_1 = 1/2\left(\begin{smallmatrix} 0 & -\overline\omega(t) \\ \overline\omega(t) & 0 \end{smallmatrix}\right)$ and $\mathcal{D}_1 = \left(\begin{smallmatrix} -\alpha/2-\gamma_1 & \gamma_2 \\ \gamma_2 & -\alpha/2+\gamma_1 \end{smallmatrix}\right)$.

Proof

$$\frac{\mathrm{d}\bar{\mathbf{u}}_h}{\mathrm{d}t} = \frac{\mathrm{d}}{\mathrm{d}t}\begin{pmatrix} V_1 & \mathbf{b}^T \\ \mathbf{l} & \alpha \end{pmatrix}\mathbf{x} = \frac{\mathrm{d}}{\mathrm{d}t}(\mathcal{D}_1\mathbf{x}_h + \Omega_1\mathbf{x}_h + \mathbf{b}z)$$

$$= \frac{\mathrm{d}}{\mathrm{d}t}\mathcal{D}_1\mathbf{x}_h + \frac{\mathrm{d}}{\mathrm{d}t}\Omega_1\mathbf{x}_h + \frac{\mathrm{d}}{\mathrm{d}t}\mathbf{b}z + (V_1 \ \mathbf{b})\begin{pmatrix} V_1 & \mathbf{b} \\ \mathbf{l}^T & \alpha \end{pmatrix}\mathbf{x}$$

$$= \frac{d}{dt}\mathcal{D}_1\mathbf{x}_h + \frac{d}{dt}\Omega_1\mathbf{x}_h + \frac{d}{dt}\mathbf{b}z + (V_1^2 + \mathbf{bl}^T)\mathbf{x}_h + (V_1 + \alpha I)\mathbf{b}z$$

$$= (-\mathcal{D}_1^2 - \Omega_1^2 - \frac{1}{2}(\mathbf{bl}^T + \mathbf{lb}^T) - \frac{f}{2}(V_1^\perp + (V_1^\perp)^T) - P_1)\mathbf{x}_h$$

$$+ (-\mathcal{D}_1\Omega_1 - \Omega_1\mathcal{D}_1 - \frac{1}{2}(\mathbf{bl}^T - \mathbf{lb}^T) - \frac{f}{2}(V_1^\perp - (V_1^\perp)^T)\mathbf{x}_h$$

$$+ (-P_2 - (V_1 + \alpha I)\mathbf{b} - f(\mathbf{b})^\perp)z + (V_1^2 + \mathbf{bl}^T)\mathbf{x}_h + (V_1 + \alpha I)\mathbf{b}z$$

$$= -f\bar{\mathbf{u}}_h^\perp - (P_1\ P_2)\mathbf{x}$$

$$\Rightarrow \frac{d\bar{\mathbf{u}}_h}{dt} + f\mathbf{u}_h^\perp = -\nabla_h p.$$

Then the first equation (A.12a) is proven. The second and third equations (A.12b) and (A.12c) are both obvious. This finishes the proof. ∎

Appendix B

As in (34), $\mathbf{X}$ is a linear transformation of ξ, and we have the following relations between the derivatives by time-ordered exponential

$$\begin{pmatrix} \partial_{\xi_1} \\ \partial_{\xi_2} \\ \partial_{\xi_3} \end{pmatrix} = \left(e^{\int_0^t A(s)ds} \right)^T \begin{pmatrix} \partial_x \\ \partial_y \\ \partial_z \end{pmatrix}, \quad \begin{pmatrix} \partial_x \\ \partial_y \\ \partial_z \end{pmatrix} = \left(\left(e^{\int_0^t A(s)ds} \right)^T \right)^{-1} \begin{pmatrix} \partial_{\xi_1} \\ \partial_{\xi_2} \\ \partial_{\xi_3} \end{pmatrix}. \tag{B.1}$$

To analyze (33), we set

$$\omega = \widehat{\omega}_\mathbf{k}(t)e^{i\mathbf{k}\cdot\xi} = \widehat{\omega}_\mathbf{k}(t)e^{i(k_1\xi_1 + k_2\xi_2 + k_3\xi_3)}. \tag{B.2}$$

Then,

$$\omega = \triangle_h\Psi = \sum_{i,j=1}^3 \left(\frac{\partial\xi_i}{\partial x}\frac{\partial\xi_j}{\partial x} + \frac{\partial\xi_i}{\partial y}\frac{\partial\xi_j}{\partial y} \right) \frac{\partial^2\Psi}{\partial\xi_i\partial\xi_j},$$

$$\Psi = \frac{-1}{\sum_{i,j=1}^3 \left(\frac{\partial\xi_i}{\partial x}\frac{\partial\xi_j}{\partial x} + \frac{\partial\xi_i}{\partial y}\frac{\partial\xi_j}{\partial y} \right)k_ik_j}\omega, \tag{B.3}$$

and

$$-\frac{\partial}{\partial z}\frac{\partial}{\partial y}\Psi = -\sum_{i,j=1}^3 \frac{\partial\xi_i}{\partial z}\frac{\partial\xi_j}{\partial y}\frac{\partial^2\Psi}{\partial\xi_i\partial\xi_j} = -\frac{\sum_{i,j=1}^3 \frac{\partial\xi_i}{\partial z}\frac{\partial\xi_j}{\partial y}k_ik_j}{\sum_{i,j=1}^3 \left(\frac{\partial\xi_i}{\partial x}\frac{\partial\xi_j}{\partial x} + \frac{\partial\xi_i}{\partial y}\frac{\partial\xi_j}{\partial y} \right)k_ik_j}\omega,$$

$$\frac{\partial}{\partial z}\frac{\partial}{\partial x}\Psi = \sum_{i,j=1}^3 \frac{\partial\xi_i}{\partial z}\frac{\partial\xi_j}{\partial x}\frac{\partial^2\Psi}{\partial\xi_i\partial\xi_j} = \frac{\sum_{i,j=1}^3 \frac{\partial\xi_i}{\partial z}\frac{\partial\xi_j}{\partial x}k_ik_j}{\sum_{i,j=1}^3 \left(\frac{\partial\xi_i}{\partial x}\frac{\partial\xi_j}{\partial x} + \frac{\partial\xi_i}{\partial y}\frac{\partial\xi_j}{\partial y} \right)k_ik_j}\omega. \tag{B.4}$$

We also have

$$J(\Psi(\mathbf{x}, t), \omega(\mathbf{x}, t)) = \nabla_h^\perp \Psi \cdot \nabla_h \omega$$

$$= \begin{pmatrix} -\dfrac{\partial \xi_1}{\partial y} & -\dfrac{\partial \xi_2}{\partial y} & -\dfrac{\partial \xi_3}{\partial y} \\[2mm] \dfrac{\partial \xi_1}{\partial x} & \dfrac{\partial \xi_2}{\partial x} & \dfrac{\partial \xi_3}{\partial x} \end{pmatrix} \nabla_\xi \Psi \cdot \begin{pmatrix} \dfrac{\partial \xi_1}{\partial x} & \dfrac{\partial \xi_2}{\partial x} & \dfrac{\partial \xi_3}{\partial x} \\[2mm] \dfrac{\partial \xi_1}{\partial y} & \dfrac{\partial \xi_2}{\partial y} & \dfrac{\partial \xi_3}{\partial y} \end{pmatrix} \nabla_\xi \omega$$

$$= -\mathbf{k}^T \Psi \begin{pmatrix} 0 & \dfrac{\partial \xi_1}{\partial x}\dfrac{\partial \xi_2}{\partial y} - \dfrac{\partial \xi_2}{\partial x}\dfrac{\partial \xi_1}{\partial y} & \dfrac{\partial \xi_1}{\partial x}\dfrac{\partial \xi_3}{\partial y} - \dfrac{\partial \xi_3}{\partial x}\dfrac{\partial \xi_1}{\partial y} \\[3mm] -\dfrac{\partial \xi_1}{\partial x}\dfrac{\partial \xi_2}{\partial y} + \dfrac{\partial \xi_2}{\partial x}\dfrac{\partial \xi_1}{\partial y} & 0 & \dfrac{\partial \xi_2}{\partial x}\dfrac{\partial \xi_3}{\partial y} - \dfrac{\partial \xi_3}{\partial x}\dfrac{\partial \xi_2}{\partial y} \\[3mm] -\dfrac{\partial \xi_1}{\partial x}\dfrac{\partial \xi_3}{\partial y} + \dfrac{\partial \xi_3}{\partial x}\dfrac{\partial \xi_1}{\partial y} & -\dfrac{\partial \xi_2}{\partial x}\dfrac{\partial \xi_3}{\partial y} + \dfrac{\partial \xi_3}{\partial x}\dfrac{\partial \xi_2}{\partial y} & 0 \end{pmatrix} \mathbf{k}\omega = 0,$$

which can be easily verified. Plugging these terms into the vorticity-stream formulation (33a), we have the following formula for the amplitude $\widehat{\omega}_\mathbf{k}(t)$

$$\frac{\mathrm{d}}{\mathrm{d}t}\widehat{\omega}_\mathbf{k}(t) = (\alpha - S(t, \mathbf{k}))\widehat{\omega}_\mathbf{k}(t), \tag{B.5}$$

with

$$S(t, \mathbf{k}) = \frac{\sum_{i,j=1}^3 \left(l_1 \dfrac{\partial \xi_i}{\partial z}\dfrac{\partial \xi_j}{\partial x} + l_2 \dfrac{\partial \xi_i}{\partial z}\dfrac{\partial \xi_j}{\partial y} \right) k_i k_j}{\sum_{i,j=1}^3 \left(\dfrac{\partial \xi_i}{\partial x}\dfrac{\partial \xi_j}{\partial x} + \dfrac{\partial \xi_i}{\partial y}\dfrac{\partial \xi_j}{\partial y} \right) k_i k_j}, \tag{B.6}$$

where each derivative term, for example $\partial \xi_i / \partial x$, is an element of the ordered exponential $(\mathrm{e}^{\int_0^t A(s)\mathrm{d}s})^T$ in (B.1).